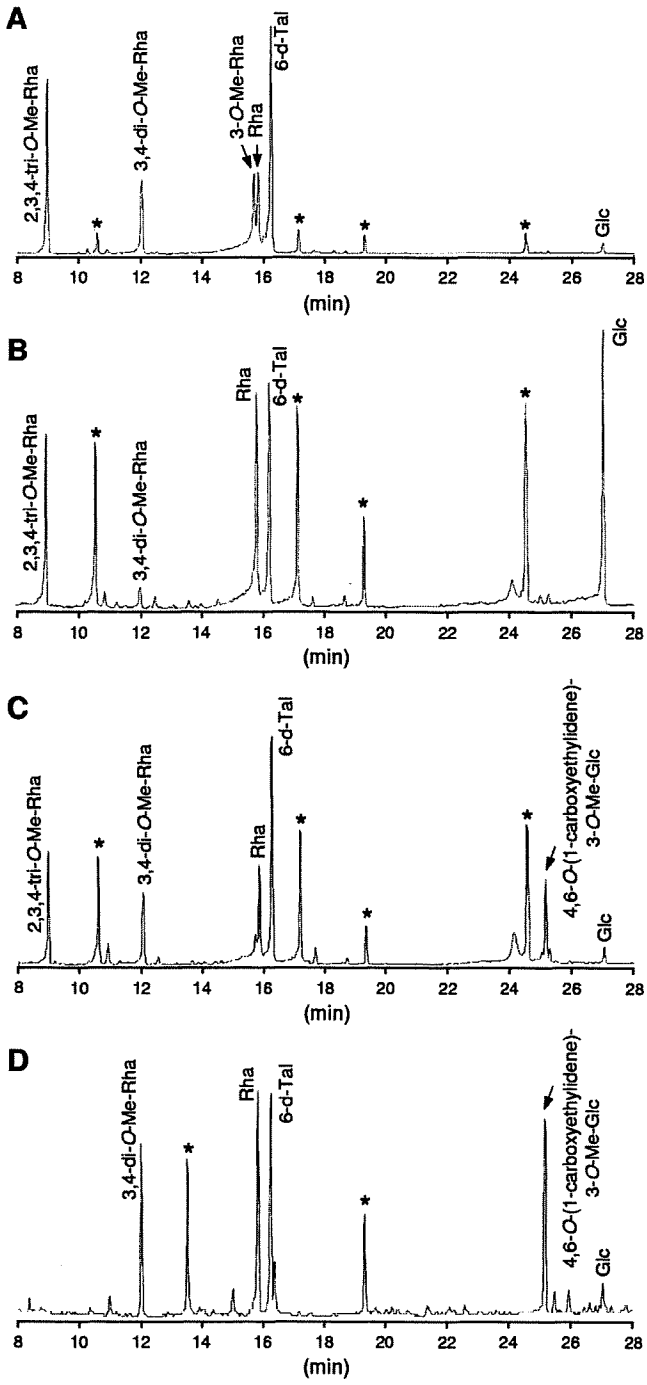


FIG. 3. GC-MS of alditol acetate derivatives from crude GPL extracts of recombinant strains *M. smegmatis* MS-S1/pYM301a (A), MS-S1/pYM-gtfTB (B), and MS-S1/pYM-gtfTB-orf3-orf4 (C) and a MAC serovar 8 strain (D). GPL extracts were prepared from the total-lipid fraction, and this was followed by mild alkaline hydrolysis. Asterisks indicate noncarbohydrates. Me, methyl.

MS-S1/pYM-gtfTB (Fig. 2, lane B). After extraction of the products from the corresponding bands on the TLC plate, purified GPL-SG-U and -D were subjected to perdeuteriomethylation followed by GC-MS. The differences in the TLC profiles of GPL-SG-U and -D might have been due to the presence or absence of fatty acid methylation, which is often observed in *M. smegmatis* GPLs (23, 31), whereas the GC-MS profiles and fragmentation ions for GPL-SG-U and -D were identical, demonstrating that GPL-SG-U and -D had the same sugar moieties and linkages. Therefore, the profiles of GPL-SG-U shown here are representative of GPL-SG-U and -D. The GC-MS profile of GPL-SG-U contained four peaks corresponding to 6-d-Tal, Rha, Glc, and 2,3,4-tri-*O*-methyl-Rha (data not shown). The characteristic spectra for Glc, Rha, and 6-d-Tal are shown in Fig. 4. The spectrum of Glc had fragment ions at *m/z* 121, 167, and 168, which represent the presence of deuteriomethyl groups at positions C-2, C-3, and C-4 (Fig. 4A). In contrast, fragment ions at *m/z* 121, 134, 193, and 240 were detected for Rha, indicating that a deuteriomethyl group was introduced at positions C-2 and C-4 of Rha, in which position C-3 was acetylated (Fig. 4B). In addition, detection of fragment ions at *m/z* 134, 181, and 193 (Fig. 4C) revealed that there was deuteriomethylation at positions C-3 and C-4 in 6-d-Tal. These results demonstrated that position C-1 of Glc is linked to position C-3 of Rha but not to position C-2 of 6-d-Tal, because it has been determined previously that position C-1 of Rha is linked to position C-2 of 6-d-Tal in the oligosaccharide of serovar 1-specific GPL (17). Accordingly, the oligosaccharide structures of GPL-SG-U and -D were determined to have Glc-(1→3)-Rha-(1→2)-6-d-Tal at D-*allo*-Thr, demonstrating that *gtfTB* encodes the glucosyltransferase that transfers a Glc residue via 1→3 linkage to the Rha residue of serovar 1-specific GPL.

**Structural assignment of GPL-S8 synthesized by expression of *gtfTB*, ORF3, and ORF4.** GC-MS of the crude GPL extract from MS-S1/pYM-gtfTB-orf3-orf4 revealed the presence of 4,6-*O*-(1-carboxyethylidene)-3-*O*-methyl-Glc (Fig. 3C). To confirm that this structural component was derived from GPL-S8, we performed GC-MS and MALDI-TOF MS analyses of purified GPL-S8. The results showed that GPL-S8 contained a 4,6-*O*-(1-carboxyethylidene)-3-*O*-methyl-Glc residue and two main pseudomolecular ions (*m/z* 1,565.9 and 1,579.8 $[M + Na]^+$) (data not shown). Consequently, as shown in Fig. 5, these results were consistent with the proposed structure for GPL-S8-1 and -2 containing 4,6-*O*-(1-carboxyethylidene)-3-*O*-methyl-Glc, with differences in pseudomolecular ions due to fatty acid methylation.

## DISCUSSION

Structural diversity of the ssGPLs, notably in their sugar residues, defines 28 serovars of MAC. Although these ssGPLs are known to contribute to the virulence of MAC, the mechanisms of their biosynthetic regulation are largely unknown. In this study, we clarified the biosynthetic pathway for serovar 8-specific GPL, specifically the glycosylation step in which a Glc residue is transferred to the Rha residue of serovar 1-specific GPL.

To isolate the genomic region associated with the biosynthesis of serovar 8-specific GPL, we compared the GPL biosynthetic gene clusters in several MAC strains and found significant differences in the *gtfB-drrC* region. The segment flanking the 3′ end of the *gtfB-drrC* region includes several genes responsible for the serovar 1-specific GPL whose structure is found in all ssGPLs. On the other hand, it is experimentally

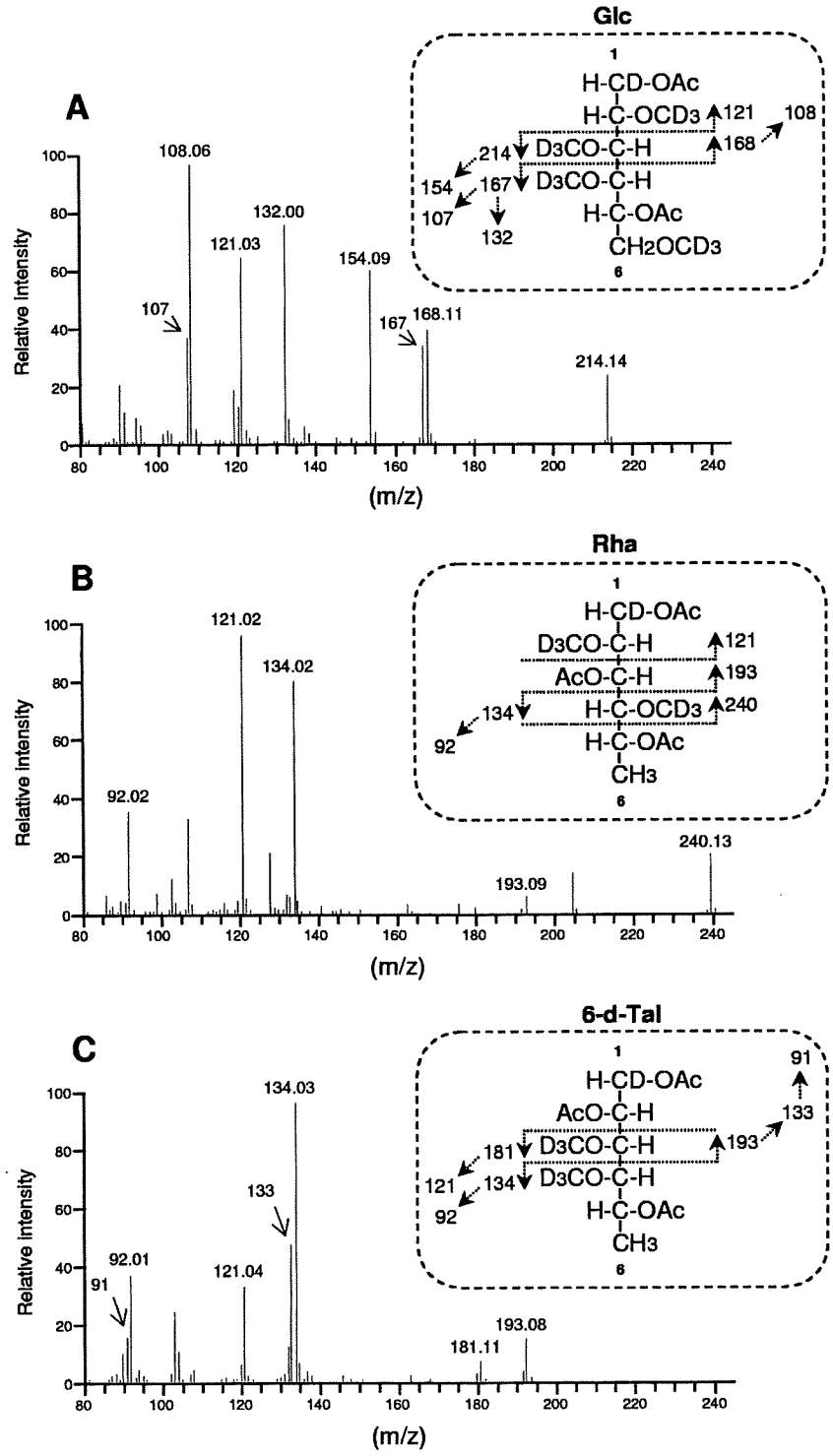


FIG. 4. GC-MS spectra and fragment ion assignments for Glc (A), Rha (B), and 6-d-Tal (C), which were derived from alditol acetates of sugars released from deuteriomethylated GPL-SG-U. Ac, acetate; D, deuterium.

clarified that the *gtfB-drrC* regions of serovar 2-, 7-, and 16-specific GPL-producing strains contain the genes involved in the formation of the specific sugar residues that are transferred to the Rha residue of serovar 1-specific GPL (18, 19, 30). Thus, this region could play an important role in generating the structural diversity of ssGPLs. As shown in this study, the specific functions for formation of sugar moieties of serovar 8-specific GPL were due to the genes present in the *gtfB-drrC*

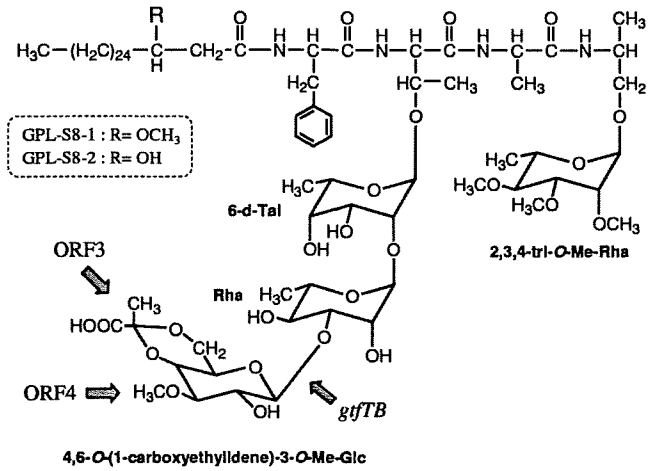


FIG. 5. Proposed structure and biosynthetic genes of GPL-S8 (serovar 8-specific GPL). Me, methyl.

region, suggesting that focusing on this region might provide clues for elucidating the characteristics of other ssGPLs whose biosynthesis is still not known.

It has been reported previously that the *gtfTB* gene in *M. avium* strains 104 and A5 was not likely to be associated with GPL biosynthesis because its ancestral homologue, Rv1516c (61% identity with the GtfTB gene), was the gene of *M. tuberculosis*, which produces no GPLs (28). Thus, it was interesting that *gtfTB* encodes a glycosyltransferase that does participate in GPL biosynthesis in which a Glc residue is transferred to serovar 1-specific GPL, yielding the serovar 8-specific GPL. *M. avium* strains 104 and A5 synthesize serovar 1-specific GPL as a final product and intermediate, respectively, while it has been recognized that neither of these strains produces serovar 8-specific GPL in spite of the presence of *gtfTB* in the GPL biosynthetic gene cluster (28). These observations raised the possibility that the transcription of *gtfTB* is inefficient in both strains due to the upstream sequences. Actually, in *M. avium* strain 104, a transposase sequence was observed upstream of *gtfTB*, indicating that this strain might be deficient in glucosylation, and consequently a serovar 1-specific GPL-producing strain is obtained (28). On the other hand, it has been shown that the biosynthetic gene cluster for serovar 7-specific GPL in *M. intracellulare* strain ATCC 35847 contains a putative glycosyltransferase gene which encodes amino acid sequences that are similar to the amino acid sequences encoded by *gtfTB* (59% identity) (18). Structural analysis of sugar moieties in serovar 7-specific GPL indicated that this GtfTB homologue may serve as a glycosyltransferase during formation of the terminal amidohexose residue that structurally resembles Glc (18).

The deduced amino acid sequences encoded by ORF3 and ORF4 showed that these genes putatively encode polysaccharide pyruvyltransferase and *O*-methyltransferase, respectively. Expression of ORF3 and ORF4 together with *gtfTB* led to structural alterations in which Glc was modified with both 4,6-*O*-(1-carboxyethylidene) and 3-*O*-methyl groups. Based on these observations, it is strongly suggested that ORF3 is associated with the formation of the 4,6-*O*-(1-carboxyethylidene) group that is synonymous with the cyclic pyruvate ketal and that ORF4 is associated with the 3-*O*-methylation of the Glc residue (Fig. 5). In mycobacteria, homologues of ORF3 and ORF4 were found only in *M. smegmatis*, as MSMEG_4736 (for ORF3), MSMEG_4737 (for ORF3), and MSMEG_4739 (for ORF4). *M. smegmatis* also produces glycolipids containing 4,6-*O*-(1-carboxyethylidene)-3-*O*-methyl-Glc as a sugar moiety (25, 34), which suggests that both homologues participate in the synthesis of these glycolipids. Sugar residues with a 4,6-*O*-(1-carboxyethylidene) group substitution have been found in carbohydrates such as extracellular polysaccharide and N-linked glycan, which are produced by some bacteria and yeasts (1, 15, 20, 22, 26). It has been shown that an increase in 4,6-*O*-(1-carboxyethylidene)-containing sugar residues leads to enhanced viscosity of extracellular polysaccharide from *Xanthomonas* sp., which alters the cell surface properties related to cellular attachment and protection from environmental stress (10). Accordingly, in terms of the properties of serovar 8-specific GPL, the presence of the 4,6-*O*-(1-carboxyethylidene) group might influence the pathogenicity of MAC serovar 8.

With regard to the antibody reactivity, it is unclear whether serovar 8-specific antibodies react with GPL-S8 because there are minor structural differences in the methylated positions of fatty acids and the terminal Rha residue linked to the tetrapeptide between GPL-S8 and serovar 8-specific GPL of MAC. Evaluation of the antibody response to GPL-S8 using serovar 8-specific antibodies would facilitate understanding the immunoreactivity mediated by ssGPLs.

In this study, we proved that *gtfTB* and adjacent genes in the GPL biosynthetic gene cluster in MAC serovar 8 strain are responsible for the formation of a unique glucose residue in serovar 8-specific GPL (Fig. 5). In particular, *gtfTB* encodes the glucosyltransferase that plays a critical role in the pathway leading from serovar 1-specific GPL to serovar 8-specific GPL. Through further study, including generation of *gtfTB* knockout mutants of MAC serovar 8 strains, results relevant to the biosynthesis of serovar 8-specific GPL might help clarify the biological function of ssGPLs and their role in the host-pathogen relationships of MAC.

## ACKNOWLEDGMENTS

This study was supported in part by a Grant-in-Aid for Young Scientists (B) from the Ministry of Education, Culture, Science and Technology of Japan and Research on Emerging and Re-Emerging Infectious Diseases from the Ministry of Health, Labor and Welfare of Japan.

## REFERENCES

1. **Aman, P., M. McNeil, L.-E. Franzen, A. G. Darvill, and P. Albersheim.** 1981. Structural elucidation, using HPLC-MS and GLC-MS, of the acidic exopolysaccharide secreted by *Rhizobium meliloti* strain Rm1021. Carbohydr. Res. **95**:263–282.
2. **Aspinall, G. O., D. Chatterjee, and P. J. Brennan.** 1995. The variable surface glycolipids of mycobacteria: structures, synthesis of epitopes, and biological properties. Adv. Carbohydr. Chem. Biochem. **51**:169–242.
3. **Barrow, W. W., T. L. Davis, E. L. Wright, V. Labrousse, M. Bachelet, and N. Rastogi.** 1995. Immunomodulatory spectrum of lipids associated with *Mycobacterium avium* serovar 8. Infect. Immun. **63**:126–133.
4. **Belisle, J. T., K. Klaczkiewicz, P. J. Brennan, W. R. Jacobs, Jr., and J. M. Inamine.** 1993. Rough morphological variants of *Mycobacterium avium*. Characterization of genomic deletions resulting in the loss of glycopeptidolipid expression. J. Biol. Chem. **268**:10517–10523.
5. **Bhatnagar, S., and J. S. Schorey.** 2007. Exosomes released from infected macrophages contain *Mycobacterium avium* glycopeptidolipids and are proinflammatory. J. Biol. Chem. **282**:25779–25789.
6. **Bjorndal, H., C. G. Hellerqvist, B. Lindberg, and S. Svensson.** 1970. Gas-liquid chromatography and mass spectrometry in methylation analysis of polysaccharides. Angew. Chem. Int. Ed. Engl. **9**:610–619.

7. **Brennan, P. J., G. O. Aspinall, and J. E. Shin.** 1981. Structure of the specific oligosaccharides from the glycopeptidolipid antigens of serovars in the *Mycobacterium avium-Mycobacterium intracellulare-Mycobacterium scrofulaceum* complex. J. Biol. Chem. **256**:6817–6822.
8. **Brennan, P. J., H. Mayer, G. O. Aspinall, and J. E. Nam Shin.** 1981. Structures of the glycopeptidolipid antigens from serovars in the *Mycobacterium avium/Mycobacterium intracellulare/Mycobacterium scrofulaceum* serocomplex. Eur. J. Biochem. **115**:7–15.
9. **Brennan, P. J., and H. Nikaido.** 1995. The envelope of mycobacteria. Annu. Rev. Biochem. **64**:29–63.
10. **Casas, J. A., V. E. Santos, and F. Garcia-Ochoa.** 2000. Xanthan gum production under several operational conditions: molecular structure and rheological properties. Enzyme Microb. Technol. **26**:282–291.
11. **Chatterjee, D., and K. H. Khoo.** 2001. The surface glycopeptidolipids of mycobacteria: structures and biological properties. Cell. Mol. Life Sci. **58**: 2018–2042.
12. **Ciucanu, I., and F. Kerek.** 1984. A simple and rapid method for the permethylation of carbohydrates. Carbohydr. Res. **131**:209–217.
13. **Daffe, M., and P. Draper.** 1998. The envelope layers of mycobacteria with reference to their pathogenicity. Adv. Microb. Physiol. **39**:131–203.
14. **Daffe, M., M. A. Laneelle, and G. Puzo.** 1983. Structural elucidation by field desorption and electron-impact mass spectrometry of the C-mycosides isolated from *Mycobacterium smegmatis*. Biochim. Biophys. Acta **751**:439–443.
15. **D'Haeze, W., J. Glushka, R. De Rycke, M. Holsters, and R. W. Carlson.** 2004. Structural characterization of extracellular polysaccharides of *Azorhizobium caulinodans* and importance for nodule initiation on *Sesbania rostrata*. Mol. Microbiol. **52**:485–500.
16. **Eckstein, T. M., J. T. Belisle, and J. M. Inamine.** 2003. Proposed pathway for the biosynthesis of serovar-specific glycopeptidolipids in *Mycobacterium avium* serovar 2. Microbiology **149**:2797–2807.
17. **Eckstein, T. M., F. S. Silbaq, D. Chatterjee, N. J. Kelly, P. J. Brennan, and J. T. Belisle.** 1998. Identification and recombinant expression of a *Mycobacterium avium* rhamnosyltransferase gene (*rtfA*) involved in glycopeptidolipid biosynthesis. J. Bacteriol. **180**:5567–5573.
18. **Fujiwara, N., N. Nakata, S. Maeda, T. Naka, M. Doe, I. Yano, and K. Kobayashi.** 2007. Structural characterization of a specific glycopeptidolipid containing a novel *N-acyl*-deoxy sugar from *Mycobacterium intracellulare* serotype 7 and genetic analysis of its glycosylation pathway. J. Bacteriol. **189**:1099–1108.
19. **Fujiwara, N., N. Nakata, T. Naka, I. Yano, M. Doe, D. Chatterjee, M. McNeil, P. J. Brennan, K. Kobayashi, M. Makino, S. Matsumoto, H. Ogura, and S. Maeda.** 2008. Structural analysis and biosynthesis gene cluster of an antigenic glycopeptidolipid from *Mycobacterium intracellulare*. J. Bacteriol. **190**:3613–3621.
20. **Gemmill, T. R., and R. B. Trimble.** 1996. *Schizosaccharomyces pombe* produces novel pyruvate-containing N-linked oligosaccharides. J. Biol. Chem. **271**:25945–25949.
21. **Horgen, L., E. L. Barrow, W. W. Barrow, and N. Rastogi.** 2000. Exposure of human peripheral blood mononuclear cells to total lipids and serovar-specific glycopeptidolipids from *Mycobacterium avium* serovars 4 and 8 results in inhibition of TH1-type responses. Microb. Pathog. **29**:9–16.
22. **Jansson, P. E., L. Kenne, and B. Lindberg.** 1975. Structure of extracellular polysaccharide from *Xanthomonas campestris*. Carbohydr. Res. **45**:275–282.
23. **Jeevarajah, D., J. H. Patterson, M. J. McConville, and H. Billman-Jacobe.** 2002. Modification of glycopeptidolipids by an *O*-methyltransferase of *Mycobacterium smegmatis*. Microbiology **148**:3079–3087.
24. **Julander, I., S. Hoffner, B. Petrini, and L. Ostlund.** 1996. Multiple serovars of *Mycobacterium avium* complex in patients with AIDS. APMIS **104**:318–320.
25. **Kamisango, K., S. Saadat, A. Dell, and C. E. Ballou.** 1985. Pyruvylated glycolipids from *Mycobacterium smegmatis*. Nature and location of the lipid components. J. Biol. Chem. **260**:4117–4121.
26. **Kojima, N., S. Kaya, Y. Araki, and E. Ito.** 1988. Pyruvic-acid-containing polysaccharide in the cell wall of *Bacillus polymyxa* AHU 1385. Eur. J. Biochem. **174**:255–260.
27. **Krzywinska, E., S. Bhatnagar, L. Sweet, D. Chatterjee, and J. S. Schorey.** 2005. *Mycobacterium avium* 104 deleted of the methyltransferase D gene by allelic replacement lacks serotype-specific glycopeptidolipids and shows attenuated virulence in mice. Mol. Microbiol. **56**:1262–1273.
28. **Krzywinska, E., and J. S. Schorey.** 2003. Characterization of genetic differences between *Mycobacterium avium* subsp. *avium* strains of diverse virulence with a focus on the glycopeptidolipid biosynthesis cluster. Vet. Microbiol. **91**:249–264.
29. **Li, Z., G. H. Bai, C. F. von Reyn, P. Marino, M. J. Brennan, N. Gine, and S. L. Morris.** 1996. Rapid detection of *Mycobacterium avium* in stool samples from AIDS patients by immunomagnetic PCR. J. Clin. Microbiol. **34**:1903–1907.
30. **Miyamoto, Y., T. Mukai, Y. Maeda, N. Nakata, M. Kai, T. Naka, I. Yano, and M. Makino.** 2007. Characterization of the fucosylation pathway in the biosynthesis of glycopeptidolipids from *Mycobacterium avium* complex. J. Bacteriol. **189**:5515–5522.
31. **Miyamoto, Y., T. Mukai, N. Nakata, Y. Maeda, M. Kai, T. Naka, I. Yano, and M. Makino.** 2006. Identification and characterization of the genes involved in glycosylation pathways of mycobacterial glycopeptidolipid biosynthesis. J. Bacteriol. **188**:86–95.
32. **Miyamoto, Y., T. Mukai, F. Takeshita, N. Nakata, Y. Maeda, M. Kai, and M. Makino.** 2004. Aggregation of mycobacteria caused by disruption of fibronectin-attachment protein-encoding gene. FEMS Microbiol. Lett. **236**:227–234.
33. **Patterson, J. H., M. J. McConville, R. E. Haites, R. L. Coppel, and H. Billman-Jacobe.** 2000. Identification of a methyltransferase from *Mycobacterium smegmatis* involved in glycopeptidolipid synthesis. J. Biol. Chem. **275**:24900–24906.
34. **Saadat, S., and C. E. Ballou.** 1983. Pyruvylated glycolipids from *Mycobacterium smegmatis*. Structures of two oligosaccharide components. J. Biol. Chem. **258**:1813–1818.
35. **Snapper, S. B., R. E. Melton, S. Mustafa, T. Kieser, and W. R. Jacobs, Jr.** 1990. Isolation and characterization of efficient plasmid transformation mutants of *Mycobacterium smegmatis*. Mol. Microbiol. **4**:1911–1919.
36. **Stover, C. K., V. F. de la Cruz, T. R. Fuerst, J. E. Burlein, L. A. Benson, L. T. Bennett, G. P. Bansal, J. F. Young, M. H. Lee, G. F. Hatfull, S. B. Snapper, R. G. Barletta, W. R. Jacobs, Jr., and B. R. Bloom.** 1991. New use of BCG for recombinant vaccines. Nature **351**:456–460.
37. **Sweet, L., and J. S. Schorey.** 2006. Glycopeptidolipids from *Mycobacterium avium* promote macrophage activation in a TLR2- and MyD88-dependent manner. J. Leukoc. Biol. **80**:415–423.
38. **Tassell, S. K., M. Pourshafie, E. L. Wright, M. G. Richmond, and W. W. Barrow.** 1992. Modified lymphocyte response to mitogens induced by the lipopeptide fragment derived from *Mycobacterium avium* serovar-specific glycopeptidolipids. Infect. Immun. **60**:706–711.
39. **Tsang, A. Y., J. C. Denner, P. J. Brennan, and J. K. McClatchy.** 1992. Clinical and epidemiological importance of typing of *Mycobacterium avium* complex isolates. J. Clin. Microbiol. **30**:479–484.
40. **Vergne, I., and M. Daffe.** 1998. Interaction of mycobacterial glycolipids with host cells. Front. Biosci. **3**:d865–876.
41. **Yakrus, M. A., and R. C. Good.** 1990. Geographic distribution, frequency, and specimen source of *Mycobacterium avium* complex serotypes isolated from patients with acquired immunodeficiency syndrome. J. Clin. Microbiol. **28**:926–929.

# Initiation of the adaptive immune response to *Mycobacterium tuberculosis* depends on antigen production in the local lymph node, not the lungs

Andrea J. Wolf,[1,4] Ludovic Desvignes,[1] Beth Linas,[1] Niaz Banaiee,[1,7] Toshiki Tamura,[5] Kiyoshi Takatsu,[6] and Joel D. Ernst[1,2,3,4]

[1]Division of Infectious Diseases, Department of Medicine, [2]Department of Pathology, and [3]Department of Microbiology, New York University School of Medicine, New York, NY 10016
[4]Biomedical Sciences Graduate Program, University of California, San Francisco, CA 94143
[5]Department of Microbiology, Leprosy Research Center, National Institute of Infectious Disease, Tokyo 189-0002, Japan
[6]Department of Microbiology and Immunology, Division of Immunology, The Institute of Medical Science, The University of Tokyo, Tokyo 108-8639, Japan
[7]Department of Pathology, Stanford University School of Medicine, Palo Alto, CA 94305

**The onset of the adaptive immune response to *Mycobacterium tuberculosis* is delayed compared with that of other infections or immunization, and allows the bacterial population in the lungs to expand markedly during the preimmune phase of infection. We used adoptive transfer of *M. tuberculosis* Ag85B-specific CD4+ T cells to determine that the delayed adaptive response is caused by a delay in initial activation of CD4+ T cells, which occurs earliest in the local lung-draining mediastinal lymph node. We also found that initial activation of Ag85B-specific T cells depends on production of antigen by bacteria in the lymph node, despite the presence of 100-fold more bacteria in the lungs. Although dendritic cells have been found to transport *M. tuberculosis* from the lungs to the local lymph node, airway administration of LPS did not accelerate transport of bacteria to the lymph node and did not accelerate activation of Ag85B-specific T cells. These results indicate that delayed initial activation of CD4+ T cells in tuberculosis is caused by the presence of the bacteria in a compartment that cannot be mobilized from the lungs to the lymph node, where initial T cell activation occurs.**

CORRESPONDENCE
Joel D. Ernst:
joel.ernst@med.nyu.edu
OR
Kiyoshi Takatsu:
takatsuk@ims.u-tokyo.ac.jp

Abbreviation used: i.n., intranasally.

Protective immunity to tuberculosis depends on CD4+ T lymphocytes in humans and in mice (1, 2), but adaptive immune responses are unable to eradicate *Mycobacterium tuberculosis* or to provide sterile immunity. One characteristic of the adaptive immune response to tuberculosis is the long interval required for its development compared with the response to immunization or to other infections. In humans, development of adaptive immunity to tuberculosis, which is measured as a response to a tuberculin skin test, requires up to 5–6 wk after infection (3, 4), whereas in mice, the earliest antigen-specific CD4+ T cell responses require a minimum of 12 d after aerosol infection (5). Although these intervals are much longer than those required for development of adaptive immune responses to other pathogens such as *Salmonella enterica, Listeria monocytogenes, Francisella tularensis,* Influenza virus, *Leishmania major,* or *Plasmodium yoelii* sporozoites (6–12), the mechanisms that account for the delay in adaptive immune responses in tuberculosis are poorly understood. Indeed, the mechanisms that underlie the initiation of adaptive immune responses to *M. tuberculosis* are themselves poorly understood. One prior study revealed that antigen-specific CD4+ T lymphocytes did not appear in the lung-draining mediastinal lymph node until after *M. tuberculosis* had disseminated to that lymph node, indicating that, whereas *M. tuberculosis* is a lung pathogen residing in antigen-presenting cells, the adaptive immune response to *M. tuberculosis* antigens is initiated in the local lymph node (5). That study also found that bacteria and T cell recall responses appear earlier in the mediastinal lymph nodes of C57BL/6 than in C3H/HeJ mice infected with *M. tuberculosis*, but it did not address the mechanisms of

The online version of this article contains supplemental material.

JEM © The Rockefeller University Press $30.00
Vol. 205, No. 1, January 21, 2008 105–115 www.jem.org/cgi/doi/10.1084/jem.20071367



Supplemental Material can be found at:
http://www.jem.org/cgi/content/full/jem.20071367/DC1

dissemination of the bacteria from the lungs to the mediastinal lymph node.

We recently reported that, in addition to macrophages, dendritic cells are infected with *M. tuberculosis* with high frequency in the lungs and mediastinal lymph node of mice, and we reported evidence that dendritic cells transport *M. tuberculosis* from the lungs to the mediastinal lymph node (13). In these studies, we used adoptive transfer of $CD4^+$ T cells that express a transgenic T cell antigen receptor specific for a peptide from *M. tuberculosis* Antigen 85B to characterize the spatial and temporal determinants of initiation of the adaptive immune response to *M. tuberculosis*. We found that activation of $CD4^+$ T cells in the mediastinal lymph node is the limiting step in development of the adaptive immune response, and that after initial proliferation in the lymph node, effector $CD4^+$ T cells traffic rapidly to the lungs. We also found that initial $CD4^+$ T cell responses depend on the presence of bacteria in the mediastinal lymph node, and that before dissemination in the lymph node, the bacteria are in a compartment in the lungs that cannot be mobilized to the lymph node by an additional proinflammatory stimulus. These findings indicate that initiation of an adaptive immune response to *M. tuberculosis* depends on transport of live bacteria from the lungs to the mediastinal lymph node, and that *M. tuberculosis* may delay this process to expand the bacterial population in the lungs and to evade immune effector mechanisms and establish chronic infection.

## RESULTS

### The adaptive immune response to *M. tuberculosis* in the lungs is delayed and has limited efficacy

In wild-type C57BL/6 mice infected by the aerosol route, *M. tuberculosis* grows progressively in the lungs for ~17–19 d (Fig. 1). Coincident with the appearance of a detectable adaptive immune response, the bacterial population stops expanding, and reaches a stable plateau. IFNγ, which is primarily produced by $CD4^+$ T cells, is one measure of adaptive immunity to *M. tuberculosis*, and its expression in the lungs coincides with the appearance of $CD4^+$ and $CD8^+$ T lymphocytes (not depicted) and with control of bacterial growth (Fig. 1). During the time required for appearance of an adaptive immune response to *M. tuberculosis* in the lungs, the bacterial population expanded >20,000-fold, and although the adaptive immune response is capable of arresting progressive growth of the bacteria, it does not lead to apparent bacterial killing.

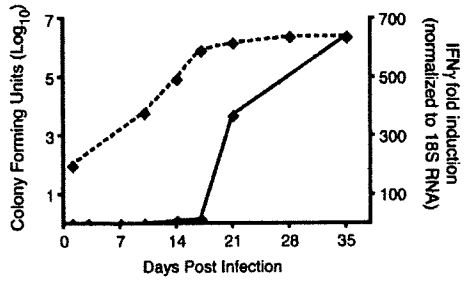


**Figure 1. Timing of the appearance of adaptive immunity compared with bacterial growth in the lungs of *M. tuberculosis*–infected C57BL/6 mice.** C57BL/6 mice were infected by the aerosol route with 50 cfu of *M. tuberculosis* (H37Rv). At designated time points, the lungs were removed and assayed for bacteria by plating and for IFNγ gene expression by real-time RT-qPCR. Four mice were assayed at each time point. Error bars represent the SEM.

The long interval between infection and appearance of adaptive immunity to *M. tuberculosis* could be attributable to delayed priming of naive antigen-specific T lymphocytes, or to delayed trafficking of effector T lymphocytes to the site of infection. To determine the contributions of these two steps to the time required for appearance of *M. tuberculosis*–specific T lymphocytes in the lungs, we used $CD4^+$ T lymphocytes from transgenic mice that express a T-cell antigen receptor, termed P25TCR-Tg, which is specific for peptide 25 (aa 240–254) of *M. tuberculosis* Antigen 85B.

### P25TCR-Tg $CD4^+$ T cells recognize Antigen 85B produced by *M. tuberculosis*

We first assessed the ability of P25TCR-Tg $CD4^+$ T cells to respond to antigen presented by cultured cells. Splenocytes from P25TCR-Tg mice stimulated with peptide antigen (peptide 25) and whole Antigen 85B (Ag85B) responded in a dose-dependent manner with maximal responses achieved at 10 μg/ml for both peptide 25 and native Ag85 isolated from *M. tuberculosis* (Fig. S1, available at http://www.jem.org/cgi/content/full/jem.20071367/DC1). In addition, naive P25TCR-Tg/Rag1$^{-/-}$ $CD4^+$ T cells responded to Ag85B expressed by *M. tuberculosis* in cultured macrophages by producing IFNγ and proliferating (Fig. S1). These results confirm that P25TCR-Tg $CD4^+$ T cells are capable of sensitive detection of Ag85B produced by live, intracellular *M. tuberculosis*.

### Proliferation of Ag85B-specific $CD4^+$ T cells begins in the mediastinal lymph node, and is delayed until 11 d after infection

To characterize the time and location of *M. tuberculosis* Ag85B-specific T cell priming after *M. tuberculosis* infection in vivo, we adoptively transferred CFSE-labeled P25TCR-Tg $CD4^+$ T cells into CD45.1 congenic wild-type mice (14). After adoptive transfer, the P25TCR-Tg $CD4^+$ T cells trafficked to secondary lymphoid tissues and represented an equal percentage (1.3%) of the $CD4^+$ T cells in all of the secondary lymphoid tissues examined, as well as in the lungs and blood (unpublished data). When examined 7 or 11 d after aerosol infection with *M. tuberculosis* (~100 cfu/mouse), a single population of $CFSE^{bright}$ P25TCR-Tg $CD4^+$ T cells was detected in the lungs and mediastinal lymph node, indicating that none of the cells had proliferated (Fig. 2 A). 14 d after infection, a small percentage of the P25TCR-Tg $CD4^+$ T cells had proliferated in the mediastinal lymph node, but not in other tissues examined (lung, spleen, and inguinal lymph node). Because some P25TCR-Tg $CD4^+$ T cells had undergone up to 7 cycles of replication, we estimated that proliferation had begun (but was not completed) on day 11, assuming ~10.6 h per cell cycle (15). This was confirmed in a subsequent experiment

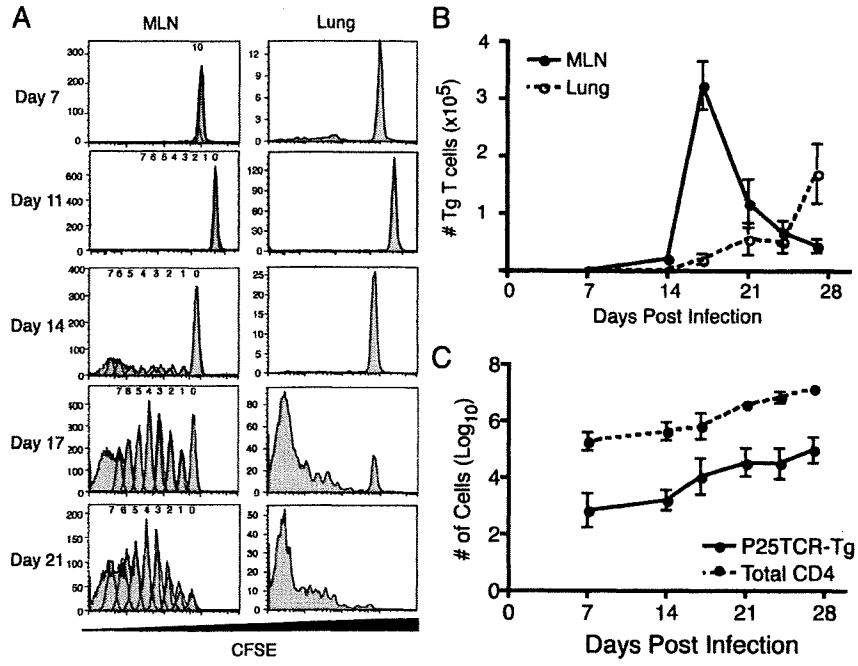


**Figure 2. Proliferation of P25TCR-Tg CD4⁺ T cells occurs in the mediastinal lymph node 11 d after infection.** (A) CFSE proliferation profile of P25TCR-Tg CD4⁺ T cells in the mediastinal lymph node and lungs over the course of the infection with *M. tuberculosis*. Plots are representative of five mice at each time point. Data from days 7, 14, 17, and 21 are from one experiment; day 11 results are from a separate experiment, using the same bacterial inoculum and number of adoptively transferred cells. (B) Total number of P25TCR-Tg CD4⁺ T cells in the mediastinal lymph node (solid line) and lung (dashed line). Replicates were averaged, and the error bars represent the SEM of five mice per time point. (C) Comparison of the number of total CD4⁺ T cells and the P25TCR-Tg CD4⁺ T cells in the lungs with time. Error bars represent the mean ± the SD.

in which ~4% of the P25TCR-Tg CD4⁺ T cells in 5 mice were in the first 2 cycles of proliferation in the mediastinal lymph node on day 12 after infection (unpublished data). By day 17 of infection, the absolute number of P25TCR-Tg CD4⁺ T cells in the mediastinal lymph node reached a peak after expanding 110-fold, and accounted for 8% of the CD4⁺ T cells in the mediastinal lymph node.

### *M. tuberculosis* Ag85B-specific CD4⁺ T cells traffic to the lungs after proliferating in the mediastinal lymph node

We also assessed Ag85B-specific T cell proliferation in the lungs. Few ($2 \times 10^5$) CD4⁺ T cells were found in the lung before infection and during the first week of infection, of which 1.03% were P25TCR-Tg CD4⁺ cells. After 14 d of infection, when T cell proliferation was detectable in the mediastinal lymph node, none of the P25TCR-Tg CD4⁺ T cells had proliferated in the lungs (Fig. 2 A). By day 17 after infection, when a high proportion of the P25TCR-Tg CD4⁺ T cells were actively proliferating in the mediastinal lymph node, P25TCR-Tg CD4⁺ T cells in the lung were either $CFSE^{high}$ or $CFSE^{low}$, with few cells of intermediate CFSE intensity. The lack of cells in the first 3 cycles of proliferation in the lungs at those time points indicates that the CFSE low-to-negative cells had migrated to the lungs after undergoing several cycles of proliferation in the lymph node. This observation is consistent with the regulation of T cell egress from the lymph node by sphingosine-1-phosphate and its receptor after initial T cell activation (16). Further evidence that Ag85B-specific CD4⁺ T cells are recruited to the lungs after proliferating in the mediastinal lymph node was provided by the observation that the total number of P25TCR-Tg CD4⁺ T cells in the lungs increases coincident with a decrease in the number of P25TCR-Tg CD4⁺ T cells in the mediastinal lymph node (Fig. 2 B). The observation that the number of P25TCR-Tg CD4⁺ T cells in the lung does not equal the number produced in the mediastinal lymph node is likely caused by the death of a large number of the cells that initially proliferated in the mediastinal lymph node (17). These observations with P25TCR-Tg CD4⁺ T cells are likely to be representative of overall *M. tuberculosis* antigen-specific CD4⁺ T cell responses, as the increases in P25TCR-Tg CD4⁺ T cells in the lung mirror the overall increase in CD4⁺ T cells in the lung (Fig. 2 C).

We considered the possibility that the delayed initial activation of P25TCR-Tg CD4⁺ T cells was a consequence of the number of cells administered because adoptive transfer of large numbers of TCR transgenic CD4⁺ T cells influences their extent of expansion (18), differentiation (19), and survival (20). However, adoptive transfer of lower numbers (in 10-fold dilutions to as low as $10^3$ cells/mouse) of P25TCR-Tg CD4⁺ T cells did not result in a detectable decrease in the time required for their initial activation after *M. tuberculosis*

infection (unpublished data). We also considered the possibility that the long interval required for activation of P25TCR-Tg CD4+ T cells was an intrinsic property of the cells, or was the consequence of the route of antigen delivery. Therefore, we examined the proliferation of P25TCR-Tg CD4+ T cells after administration of recombinant Ag85B by the respiratory and subcutaneous routes. This revealed that adoptively transferred P25TCR-Tg CD4+ T cells could respond by proliferating extensively in vivo within 3 d of immunization, irrespective of the route of antigen delivery (Fig. S2, available at http://www.jem.org/cgi/content/full/jem.20071367/DC1). These findings indicate that the delayed initial activation of P25TCR-Tg CD4+ cells in vivo after *M. tuberculosis* infection is not attributable to an artifact of the experimental system.

### P25TCR-Tg CD4+ T cell responses are specific for Antigen 85B

To characterize the specificity of P25TCR-Tg CD4+ T cells in vivo, we infected mice with an Antigen 85B–null strain of *M. tuberculosis* (Ag85BKO-Mtb). After aerosol infection, the Ag85BKO-Mtb strain grew in the lungs and disseminated to the mediastinal lymph node at a rate equivalent to that of wild-type *M. tuberculosis* H37Rv (Fig. 3 A). Nevertheless, P25TCR-Tg CD4+ T cell proliferation was not detectable in the mediastinal lymph node or in the lung, even as late as 27 d after infection (Fig. 3 B). The results demonstrate that all the P25TCR-Tg CD4+ T cell proliferation detected in vivo was Antigen 85B specific. Additionally, the lack of any response in the absence of antigen implies a lack of expansion of bystander CD4+ T cells during the initial phase of *M. tuberculosis* infection.

### Analysis of T cell activation markers and IFNγ production

We also considered the possibility that *M. tuberculosis*–specific CD4+ T cells might become partially activated earlier in infection, but that there is an abnormally long lag period between initial activation and proliferation. We therefore assessed expression of the early activation marker CD69, as well as CD25 expression on the surface of P25TCR-Tg CD4+ T cells during the course of infection. CD69 expression on P25TCR-Tg CD4+ T cells was first observed on day 12, which is approximately coincident with the beginning of measurable proliferation in the mediastinal lymph node, although 5% more of the P25TCR-Tg CD4+ T cells had up-regulated CD69 than had begun to proliferate, indicating that CD69 is up-regulated before proliferation begins (Fig. S3, available at http://www.jem.org/cgi/content/full/jem.20071367/DC1). The percentage of CD25+ P25TCR-Tg CD4+ T cells increased concurrent with the onset of proliferation in the mediastinal lymph node (Fig. S3). In addition, a small percentage (4%) of the adoptively transferred cells were competent to produce IFNγ by day 14 of infection; the percentage of IFNγ-producing P25TCR-Tg cells increased further between 14 and 17 d after infection, and was highest in cells that had undergone 4 or more cycles of cell division (Fig. S3).

Analysis of CD69 and CD25 expression on P25TCR-Tg CD4+ cells in the lungs revealed that neither of these markers

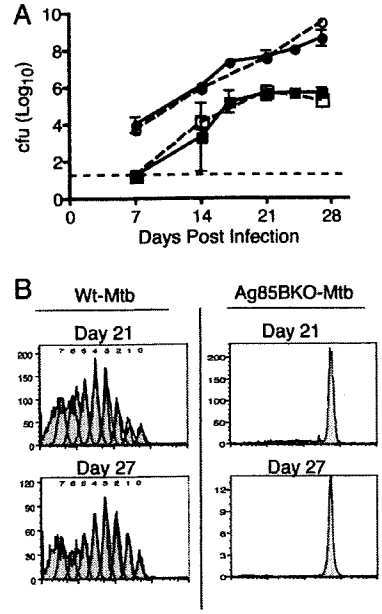


**Figure 3. P25TCR-Tg CD4+ T cell responses are specific for *M. tuberculosis* Antigen 85B.** (A) CFSE-labeled CD4+ P25TCR-Tg CD4+ T cells were adoptively transferred into C57BL/6J mice, and after 24 h, mice were infected with either wild-type *M. tuberculosis* (Wt-Mtb, solid lines) or Antigen 85BKO *M. tuberculosis* (Ag85BKO-Mtb, dashed lines with open symbols) by the aerosol route. The initial inoculum for both strains was ~100 bacteria/mouse. Total bacterial load was assessed over the first 28 d of infection in the lungs (circles) and the mediastinal lymph node (squares). At each time point, two Ag85BKO-Mtb–infected mice were assessed with a difference of <0.5 $\log_{10}$. Error bars for WT-Mtb represent the mean ± the SD of five mice. The dashed line represents the limit of detection for the cfu assay (18.75 cfu/mouse). The mediastinal lymph node cfu of all the mice at day 7 were below the limit of detection. (B) CFSE proliferation profile of P25TCR-Tg CD4+ T cells in the mediastinal lymph node.

were expressed before the appearance of cells that had previously proliferated (Fig. S3), further supporting the conclusion that initial CD4+ T cell activation occurs before recruitment to the lungs. Likewise, cells that were competent for IFNγ production did not appear in the lungs until the arrival of P25TCR-Tg CD4+ T cells that had previously proliferated (4 or more cycles) outside the lungs.

### Delayed activation of *M. tuberculosis*–specific CD4+ T cells is not solely caused by a low bacterial inoculum

Because infection with *M. tuberculosis* was routinely established with a small bacterial inoculum (~100 cfu), it is possible that one determinant of the delay in initiation of adaptive immune responses is the abundance of antigen, especially because *M. tuberculosis* replicates slowly. To assess this possibility, we infected four groups of mice by the aerosol route with a range of bacterial inocula between 15 and 700 cfu per mouse and assessed proliferation of adoptively transferred P25TCR-Tg CD4+ T cells during the first 24 d of infection. In the lungs, each inoculum resulted in a distinct bacterial burden over the

course of the infection, with a 2 $\log_{10}$ difference between the highest and lowest dose at each time point (Fig. 4 A). Varying the inoculum also resulted in a 2 $\log_{10}$ difference in bacteria in the mediastinal lymph node in mice that received the highest and lowest inocula (Fig. 4 B). This revealed that decreasing the initial inoculum below 30 cfu/mouse led to an additional 3 d delay in P25TCR-Tg CD4$^+$ T cell proliferation, whereas increasing the inoculum to 700 cfu/mouse did not lead to earlier proliferation, but caused a slight increase in the fraction of the cells that proliferated by day 14 (Fig. 4 B). These results indicate that, whereas initial activation of Ag85B-specific CD4$^+$ T cells is partially sensitive to the number of bacteria administered, the delay between initial infection and the earliest activation of CD4$^+$ T cells could not be attributed solely to the low number of bacteria used to initiate infection.

### Initial activation of *M. tuberculosis*–specific CD4$^+$ T cells is determined by the number of bacteria in the mediastinal lymph node

Because naive T lymphocytes traffic to the lungs and other peripheral tissues with low frequency, it was not surprising that activation of *M. tuberculosis*–specific T cells occurred earliest in the mediastinal lymph node. To determine whether the source of antigen for initial stimulation of Ag85B-specific CD4$^+$ T cells is in the lungs or in the mediastinal lymph node (which have ~100-fold fewer bacteria than the lungs), we tested the hypothesis that stimulation of CD4$^+$ T cells depends on the number of bacteria in the lymph node by examining the relationship between the number of bacteria in the mediastinal lymph node and proliferation of adoptively transferred P25TCR-Tg cells. We pooled the results of three independent experiments and plotted the $\log_{10}$ mediastinal lymph node cfu versus the percentage of P25TCR-Tg CD4$^+$ T cells that had proliferated in the mediastinal lymph node for each mouse. The resulting plot revealed that no proliferation occurred when there were fewer than ~1,500 cfu in the mediastinal lymph node, even when there were as many as $5 \times 10^4$ cfu in the lungs. However, once a threshold number of bacteria (1,500–3,000 per lymph node) were present in the lymph node, there was a linear correlation between cfu and the percentage of P25TCR-Tg CD4$^+$ T cells that proliferated ($r^2 = 0.77$; Fig. 4 C).

When lung cfu were plotted against the mediastinal lymph node cfu, there was little correlation between the lung cfu and the lymph node cfu in individual mice early in infection, when lung cfu were <5 $\log_{10}$ (Fig. 4 D). When we analyzed

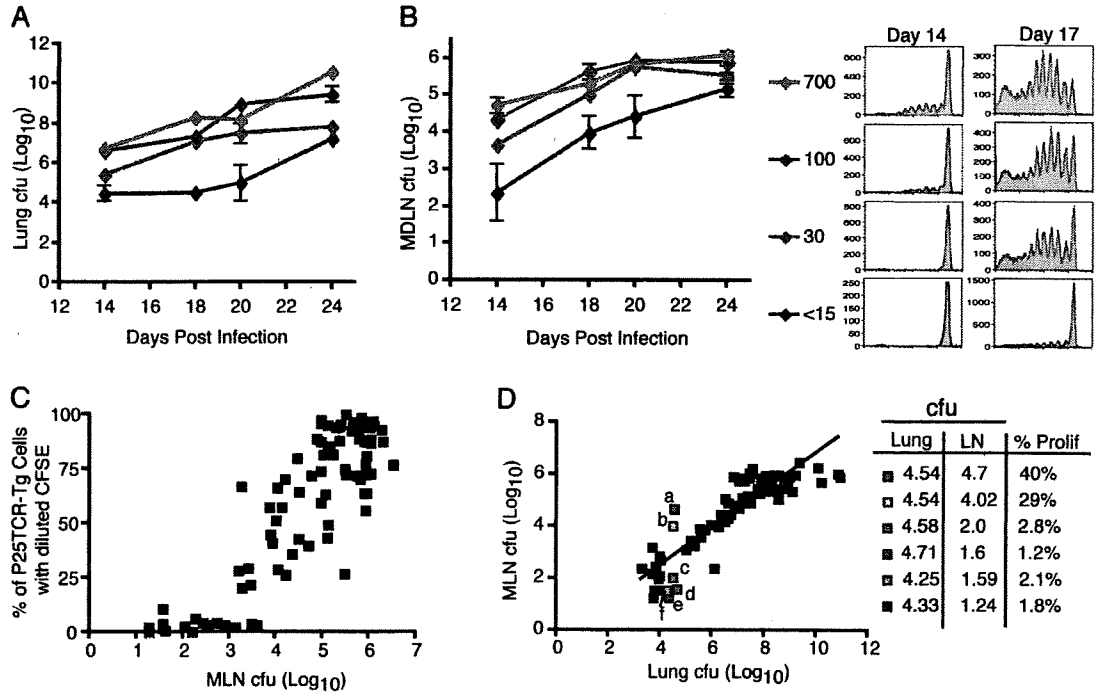


**Figure 4. Dependence of initiation of proliferation on the inoculum of *M. tuberculosis*.** Bacterial cfu in the lung (A) and mediastinal lymph node (B) over the course of the infection after inocula of <15, 30, 100, or 700 bacteria per mouse. (B) Histograms are representative of P25TCR-Tg CD4$^+$ T cell proliferation in the mediastinal lymph node 14 (left column) or 17 (right column) d after infection in mice that received the designated inocula. (C) Correlation of mediastinal lymph node bacterial burden and proliferation of P25TCR-Tg CD4$^+$ T cells. Data are from three independent experiments, and include data from mice that received distinct inocula and that were harvested on various days after infection. (D) Correlation of lung and mediastinal lymph node cfu and P25TCR-Tg CD4$^+$ T cell proliferation. Six mice with similar lung cfu and dissimilar mediastinal lymph node cfu are highlighted. Inset table shows the $\log_{10}$ lung cfu (Lung), $\log_{10}$ mediastinal lymph node cfu (LN), and the percentage of P25TCR-Tg CD4$^+$ T cells that had undergone one or more cycles of proliferation in the mediastinal lymph node for each of the highlighted mice.

a subgroup of mice with lung bacterial loads in the narrow range between 4.33 and 4.71 $\log_{10}$ cfu, individual mice exhibited a broad range (1.24–4.7 $\log_{10}$) in the number of bacteria in the mediastinal lymph node. In these mice, proliferation of P25TCR-Tg CD4$^+$ T cells also exhibited a broad variation (1.2–40%), and correlated closely with the number of bacteria in the lymph node and not in the lung. Thus, we conclude that the timing of CD4$^+$ T cell activation is tightly linked to the number of bacteria in the mediastinal lymph node.

### Delayed bacterial dissemination to the mediastinal lymph results in delayed T cell activation

We recently reported that plt mice, which lack expression of the CCR7 ligands CCL19 and CCL21ser, exhibit defective trafficking of *M. tuberculosis* from the lungs to the mediastinal lymph node (13). If initiation of CD4$^+$ T cell responses to *M. tuberculosis* depends on the number of bacteria expressing antigen in the lymph node, then plt mice should exhibit delayed activation of *M. tuberculosis*–specific CD4$^+$ T cells in the mediastinal lymph node. To test this hypothesis, we adoptively transferred CFSE-labeled P25TCR-Tg CD4$^+$ T cells into *M. tuberculosis*–infected wild-type and plt mice and assessed the timing of T cell proliferation. 14 d after infection, when antigen-specific CD4$^+$ T cell proliferation was detected in wild-type mice, 50% fewer P25TCR-Tg CD4$^+$ T cells had started to divide in plt mice at the same time point (Fig. 5 A). The reduced T cell proliferation in plt mice was accompanied by a 40% reduction in the number of bacteria in the mediastinal lymph node compared with wild-type mice at day 14 (Fig. 5 B). Overall, the CD4$^+$ T cell responses were delayed by ~3 d in plt mice.

### Ag85B-specific T cell proliferation occurs in nondraining lymph nodes and spleen if sufficient bacteria are present in the tissue

To further test the hypothesis that activation of *M. tuberculosis*–specific CD4$^+$ T cells requires production of antigen by bacteria in the lymph node, rather than occurring by transfer of soluble antigen synthesized by bacteria in the lungs, we assessed proliferation of P25TCR-Tg CD4$^+$ T cells in the inguinal lymph node, which does not receive lymphatic drainage from the lungs. This revealed that activation and proliferation of Ag85B-specific CD4$^+$ T cells could be initiated in the inguinal lymph node after aerosol infection with *M. tuberculosis* (Fig. 6 A). The timing of P25TCR-Tg CD4$^+$ T cell proliferation in the inguinal lymph node followed responses in the mediastinal lymph node by 7–10 d, and varied more from mouse to mouse than did responses in the mediastinal lymph node. Nevertheless, proliferative responses in the inguinal lymph node correlated closely with the number of bacteria present in the lymph node (Fig. 6, B and C). Additionally, we found that lymph nodes in diverse anatomical locations could be sites of proliferation of P25TCR-Tg CD4$^+$ T cells, if they contained sufficient numbers of viable *M. tuberculosis* (unpublished data). The initiation of proliferation of *M. tuberculosis*–specific CD4$^+$ T cells in lymph nodes that contain viable *M. tuberculosis*, but

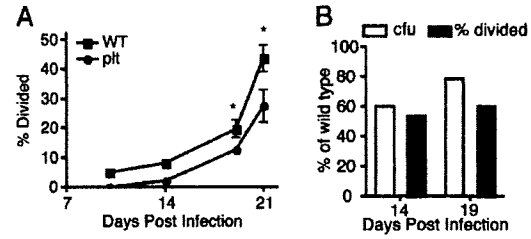


**Figure 5. Delayed dissemination of *M. tuberculosis* in plt mice results in further delayed T cell activation.** (A) Proliferation of CFSE-labeled P25TCR-Tg CD4$^+$ T cells after adoptive transfer to *M. tuberculosis*–infected wild-type C57BL/6J or plt mice. Results shown are the percentage of P25TCR-Tg CD4$^+$ T cells that had started to divide, to correct for the partial defect in the number of adoptively transferred cells that trafficked to the mediastinal lymph node of plt mice. To detect P25TCR-Tg CD4$^+$ T cells on days 10 and 14, it was necessary to pool lymph nodes from 5 mice, therefore statistical analysis was not done on those samples. Error bars on days 19 and 21 represent the mean ± the SD of 3 C57BL/6J mice and 5 plt mice. *, $P < 0.05$ by Student's *t* test. The percentage of CD69$^+$ P25TCR-Tg CD4$^+$ T cells was also fourfold lower in plt mice compared with wild-type at day 14 (not depicted). (B) Bar graph displaying the percentage of P25TCR-Tg CD4$^+$ T cells that had divided and the cfu at days 14 and 19 for the plt mice as the percentage of wild-type levels.

do not drain the lungs, further supports the conclusion that CD4$^+$ T cell activation requires synthesis of antigens in the local lymph node, and that production of *M. tuberculosis* antigens in the lungs plays little, if any, role in initiating responses of naive T lymphocytes.

In the spleen, we found that on day 14 of infection there were >10-fold fewer bacteria in the spleen compared with the mediastinal lymph node (Fig. 6 B). The difference in bacterial load narrowed over the next 2 wk of the infection. Proliferation of P25TCR-Tg CD4$^+$ T cells occurred in the spleen, but followed T cell responses in the mediastinal lymph node by ~3 d (Fig. 6 A). At the point when P25TCR-Tg CD4$^+$ T cell proliferation occurred in the spleen (day 17), the bacterial load in the spleen had reached approximately the same level as in the mediastinal lymph node when initial proliferation was detected.

### Addition of a proinflammatory stimulus does not accelerate the T cell response to live *M. tuberculosis*

The observations that the initial adaptive immune response to an *M. tuberculosis* is delayed, that activation of *M. tuberculosis*–specific CD4$^+$ T cells depends on bacterial production of antigen in the lymph node, and that the number of bacteria in the lymph node is only ~1% of that in the lung suggest that *M. tuberculosis* might impair maturation and/or trafficking of dendritic cells from the lungs to the lymph node. To test this hypothesis, we administered LPS intranasally (i.n.) to mice that had been infected with wild-type *M. tuberculosis* 10 d earlier. The administration of LPS resulted in a 12.4-fold increase in the number of myeloid dendritic cells (CD11c$^{hi}$CD11b$^{hi}$) in the lungs, and in a 12-fold increase in myeloid dendritic cells recruited to the mediastinal lymph node (Fig. 7 A). The increase

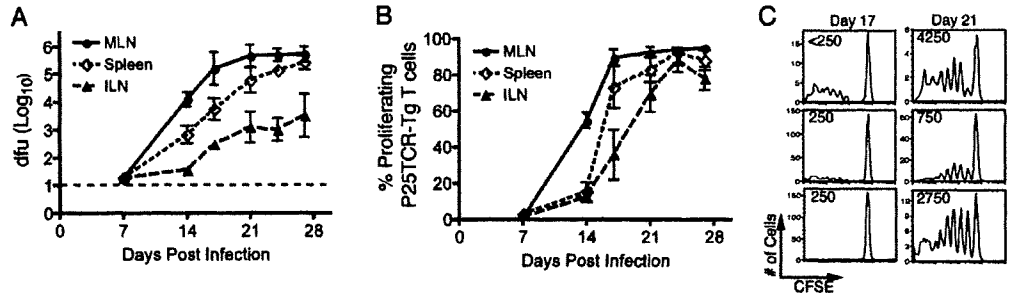


**Figure 6. *M. tuberculosis* disseminates and activates P25TCR-Tg CD4+ T cells in lymphoid tissues that do not drain the lungs.** (A) Bacterial load in the mediastinal lymph node (MLN), spleen, and inguinal lymph node (ILN) with time. The dashed line represents the limit of detection (18.75 cfu/mouse). Error bars represent the SD. (B) The percentage of P25TCR-Tg CD4+ T cells that have undergone at least 1 cycle of proliferation in the mediastinal lymph node (MLN), spleen, and inguinal lymph node (ILN). Error bars represent the SEM. (C) CFSE histograms form the inguinal lymph node at days 17 and 21 after infection; each histogram represents one mouse. Values in the top left corner represent the number of cfu found in the inguinal lymph node of that mouse.

in the number of myeloid dendritic cells was accompanied by their increased maturation, as assessed by surface expression of MHC class II (Fig. 7 B). However, despite the increased number of dendritic cells in the lungs and mediastinal lymph node, there was no increase in the number of bacteria transported to the mediastinal lymph node from the lungs (Fig. 7 C), and there was no increase in proliferation of P25TCR-Tg CD4+ T cells in the mediastinal lymph node after treatment with LPS (Fig. 7 D), unless recombinant Ag85B was coadministered with LPS (Fig. 7 E).

## DISCUSSION

The adaptive cellular immune response to *M. tuberculosis* is only partially efficacious, as it can restrict progressive growth of the bacteria, but rarely if ever eradicates them. In our studies, we used adoptive transfer of cells from transgenic mice whose CD4+ T lymphocytes express an antigen receptor specific for a peptide from *M. tuberculosis* Antigen 85B to characterize the initial events in the adaptive immune response to *M. tuberculosis*. In accord with studies that used ex vivo T cell restimulation to characterize the location and timing of CD4+ T cell responses to *M. tuberculosis*, we found that the earliest detectable responses of adoptively transferred Ag85B-specific CD4+ T cells occur in the lung-draining mediastinal lymph node, are delayed until 10–12 d after infection, and are preceded by the appearance of live *M. tuberculosis* in the mediastinal lymph node. In addition, we found strong evidence that activation of Ag85B-specific CD4+ T cells depends on the number of *M. tuberculosis* in the lymph node rather than in the lungs. We also found that transfer of *M. tuberculosis* from the lungs to the lymph node could not be accelerated by pulmonary administration of LPS, indicating that early in infection, the bacteria are in a compartment that is not competent to migrate, suggesting that slow growth of *M. tuberculosis* in the lungs does not fully account for delayed T cell activation. Collectively, these results indicate that during early stages of infection in vivo, *M. tuberculosis* occupies one or more compartments that do not promote antigen presentation to naive CD4+ T cells, and this allows dramatic expansion of the bacterial population in the lungs. We propose that this allows the large bacterial population to resist effector mechanisms of the adaptive immune response, and allows *M. tuberculosis* to persist in the lungs.

Antigen 85B is an abundant secreted protein of *M. tuberculosis* that represents >20% of the protein in culture filtrates, and is expressed and secreted by *M. tuberculosis* within host cells (21, 22). As a secreted protein and frequent target of immune responses in humans (23) and mice, Ag85B has been considered to be a potential candidate vaccine antigen, and a recombinant BCG strain that overproduces Ag85B is currently being prepared for human clinical trials. Because Ag85B is secreted, has been observed in extraphagosomal vesicles of macrophages (22), and expression has been detected in the lungs early during infection (24), we expected that production and secretion of Ag85B by *M. tuberculosis* in the lungs would be sufficient to deliver soluble antigen to activate Ag85B-specific CD4+ T cells in the local draining lymph node. If this were the case, Ag85B-specific T cell responses in the lymph node should directly correlate with the number of bacteria in the lungs. Instead, we found that although the number of bacteria in the lungs increases progressively during the first 2–3 wk of infection, Ag85B-specific CD4+ T cell responses were not observed until a threshold number of viable bacteria (~1,500–3,000) appeared in the mediastinal lymph node. Moreover, although the number of bacteria in the lymph node in most mice was closely related to (and ~100-fold less than) the number of bacteria in the lungs, analysis of several mice with discordant bacterial burdens in the lungs and lymph node revealed that responses of Ag85B-specific CD4+ T cells correlated with the number of bacteria in the mediastinal lymph node, and not with the number of bacteria in the lungs. Additional evidence that production of Ag85B by live bacteria in the lymph node is essential to initiate T cell responses in the context of *M. tuberculosis* infection was provided by analysis of Ag85B-specific CD4+ T cell responses in lymph nodes that do not drain the lungs. This analysis revealed that Ag85B-specific CD4+ T cell responses occurred in peripheral (nonlung draining) lymph nodes as long as a sufficient number of live bacteria were present in the same

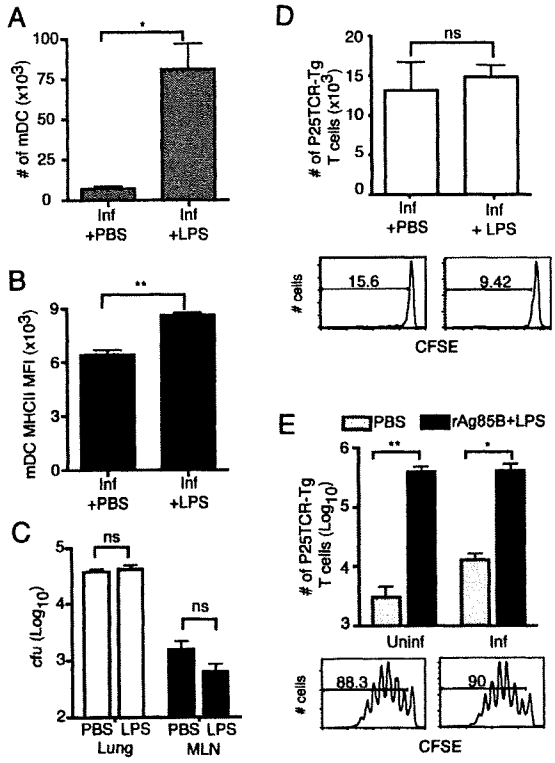


**Figure 7. Airway administration of LPS does not increase translocation of *M. tuberculosis* from the lungs to the mediastinal lymph node, and does not accelerate P25TCR-Tg CD4⁺ T cell responses.** Mice that were either uninfected or infected 10 d earlier with wild-type *M. tuberculosis* received 5 × $10^6$ CFSE-labeled P25TCR-Tg CD4⁺ T cells 4 d before harvest. 24 h later, i.e., 3 d before harvest, mice were given sterile PBS or 1 μg LPS with or without 50 ng of recombinant Antigen 85B (rAg85B) by the intranasal route. (A) The number of myeloid dendritic cell in the mediastinal lymph node. (B) Surface MHC class II mean fluorescence intensity (MFI) on mediastinal lymph node myeloid dendritic cell. (C) Cfu in the lung and mediastinal lymph node (MLN) in mice infected with wild-type *M. tuberculosis* that either received PBS or LPS i.n. (D) Change in the number of P25TCR-Tg CD4⁺ T cells caused by proliferation as assessed in the mediastinal lymph node at day 14 after infection (4 d after LPS or control). Histograms show day 14 CFSE proliferation profiles of representative mice given either PBS (D, left) or LPS (D, right) i.n. (E) Comparison of the number of P25TCR-Tg CD4⁺ T cells in the mediastinal lymph node of uninfected or *M. tuberculosis*–infected mice that received either PBS or rAg85B + LPS i.n. Histograms represent the proliferation profile of the CFSE-labeled P25TCR-Tg cells in uninfected + rAg85B + LPS (left) and infected + rAg85B + LPS (right). The number of cells was determined by multiplying the percentage as determined by flow cytometry by the total number of cells in the lymph node as assessed by trypan exclusion. Three mice were examined per group, and the error bars represent the SD. Statistics were done using Student *t* test. *, $P < 0.05$; **, $P < 0.01$. ns, not significant.

lymph node. These results indicate that, even for an abundant secreted protein antigen, stimulation of CD4⁺ T cells requires short-range interactions between *M. tuberculosis*–infected cells and antigen-specific T cells.

We considered the possibility that the immune response to *M. tuberculosis* Ag85B is aberrant or otherwise unrepresentative of *M. tuberculosis* antigens. However, we found that the temporal and quantitative characteristics of expansion of adoptively transferred Ag85B-specific CD4⁺ T cells paralleled that of total CD4⁺ T cell responses during the course of *M. tuberculosis* infection (Fig. 2). Moreover, our results correspond closely to those obtained by ex vivo restimulation with an *M. tuberculosis* lysate (5).

The observation that initial Ag85B-specific CD4⁺ T cell responses require the presence of live bacteria in the lymph node suggests that the time required for *M. tuberculosis* to enter a compartment that is competent for transport to the local lymph node may account for the delay in initiation of the adaptive immune response in tuberculosis. Although slow replication of *M. tuberculosis* could be assumed to account for the delayed cellular immune response, our data imply that slow bacterial growth cannot fully explain the temporal characteristics of the immune response. If a simple model of slow growth accounted for insufficient antigen for CD4⁺ T cell activation, the time required to initiate the immune response should be reduced by a higher inoculum of bacteria. For example, increasing the inoculum from 100 to 700 bacteria/mouse in the initial inoculum should have reduced the time dependence of Ag85B-specific CD4⁺ T cell activation by ~2.6 bacterial doubling times (71 h, based on the growth curve shown in Fig. 1). Instead, we found no difference in the time required to initiate proliferation of Ag85B-specific CD4⁺ T cells in mice infected with 100 or 700 bacteria, which implies that one or more factors other than a low initial inoculum contribute to the long interval preceding Ag85B-specific CD4⁺ T cell responses.

We recently reported that, after aerosol infection of mice with *M. tuberculosis*, myeloid dendritic cells become infected in the lungs, and represent the predominant cells that contain *M. tuberculosis* in the mediastinal lymph node (13). Moreover, we found that plt mice exhibited a parallel decrease in dendritic cell recruitment and dissemination of *M. tuberculosis* to the mediastinal lymph node. These results provide evidence that myeloid dendritic cells become infected in the lungs and transport live *M. tuberculosis* to the local lymph node. Together with the observation that plt mice also show an increased delay in activation of Ag85B-specific CD4⁺ T cells (Fig. 5), these results suggest that myeloid dendritic cell transport of *M. tuberculosis* to the local lymph node is a critical determinant of the initiation of the adaptive immune response in tuberculosis.

Because transport of *M. tuberculosis* to the mediastinal lymph node was not apparent until 11–12 d after infection, we tested the hypothesis that administration of lipopolysaccharide to *M. tuberculosis*–infected mice would accelerate migration of infected dendritic cells from the lungs to the mediastinal lymph node, and thereby accelerate activation of Ag85B-specific CD4⁺ T cells. Although intranasal administration of lipopolysaccharide did result in recruitment of additional macrophages and dendritic cells to the lungs of infected mice, and resulted in recruitment of additional dendritic cells to the mediastinal lymph node, this did not result

in an increase in the number of bacteria transported to the lymph node, and did not result in increased activation of Ag85B-specific CD4+ T cell responses. These results imply that during the early stage of *M. tuberculosis* infection, the bacteria are in a cellular compartment that is unable to migrate from the lungs to the lymph node. Whether the bacteria are in cells that intrinsically lack the ability to migrate, or whether they inhibit migration of dendritic cells from the lungs to the lymph node, will require further study.

The findings reported here have several implications for understanding the biology of tuberculosis. In particular, they indicate that even though the lungs are the site of infection with *M. tuberculosis*, the cellular immune response is not initiated in the lungs. This is consistent with the well-characterized trafficking patterns of naive T lymphocytes that circulate through peripheral nonlymphoid organs with low frequency (25, 26). Therefore, even though a large number of bacteria are present and a large quantity of antigen is produced by bacteria in the lungs (24), initiation of the adaptive immune response requires transport of bacteria from the lungs to the local draining lymph node or other secondary lymphoid tissues. Second, the observation that the bacterial population in the lungs expands 10,000–100,000-fold between the time of initial infection and appearance of the adaptive immune response in the lungs implies that the effector mechanisms of the adaptive immune response confront a large bacterial burden when they do appear in the lungs. Because *M. tuberculosis* has been found to inhibit cellular responses to IFNγ (27–30) and MHC class II antigen presentation (31–33), the existence of such a large bacterial population in the lungs may interfere with recognition by and/or effector functions of CD4+ T cells, and thereby inhibit the ability of the adaptive immune response to eradicate *M. tuberculosis* from the lungs. Third, these findings may provide a basis for further analysis of the differential outcomes in humans infected with *M. tuberculosis*. Although a high proportion of humans that encounter *M. tuberculosis* develop immune responses that contain the infection as latent tuberculosis, ~5% progress to active, symptomatic infection within 2 yr of initial infection (34). Although identifiable factors such as HIV infection account for some cases of progressive infection (35), most are unexplained. The findings reported here from studies of mice suggest that variations in transport of bacteria from the lungs to the local lymph node and initiation of the adaptive immune response may underlie some of the differential outcomes of *M. tuberculosis* infection in humans.

## MATERIALS AND METHODS

**Mice.** P25TCR-Tg mice, whose CD4+ T cells express a transgenic T-cell antigen receptor that recognizes peptide 25 (aa 240–254) of *M. tuberculosis* Antigen 85B bound to I-$A^b$ was prepared on a C57BL/6 background, as previously described (36). Mice for experiments were bred in the New York University School of Medicine animal facility. Genotypes of all mice were confirmed by PCR testing of tail genomic DNA. CD45.1 mice were either bred in the New York University School of Medicine animal facility or purchased from Taconic Farms, Inc. All animal experiments were done in accordance with procedures approved by the New York University School of Medicine Institutional Animal Care and Use Committee.

**Generation and characterization of Antigen 85B–deficient *M. tuberculosis*.** Antigen 85B (Rv1886c)–deficient *M. tuberculosis* mutant was created with the conditionally replicating mycobacteriophages, as previously described (37). The upper and lower allelic exchange substrates were PCR amplified from H37Rv genomic DNA and cloned into pCR2.1-TOPO (Invitrogen). The allelic exchange substrates were sequenced and directionally cloned into pYUB854. After transduction of H37Rv and plating on Middlebrook 7H9 agar supplemented with albumin-dextrose-catalase, several colonies were picked and screened for the absence of Antigen 85B mRNA by real-time RT-PCR. Antigen 85B–deficient clones (Ag85BKO-Mtb) were also examined by Western blot to confirm the absence of Antigen 85B protein using a monoclonal antibody against the Antigen 85B complex.

**Preparation and characterization of recombinant Antigen 85B.** Recombinant Antigen 85B was produced using the expression plasmid pMRLB47.Rv1886c obtained through the National Institutes of Health TB Vaccine Testing and Research Materials Contract (NIAID N01AO040091). *Escherichia coli* BL21(DE3)pLysS (Novagen) was transformed with the expression plasmid. Bacteria were grown in Lurie-Bertani broth at 37°C until $OD_{600} = 0.5$, and then the culture was shifted to 30°C in the presence of 0.5 mM IPTG. Lysis of *E. coli* and extraction of recombinant protein was done using BugBusters reagent and His-Bind kit (Novagen) according to the manufacturer's instructions, followed by dialysis in PBS and quantitation using BCA Protein Assay (Thermo Fisher Scientific). Protein purity was assessed by SDS-PAGE and Bio-Safe Coomassie staining (Bio-Rad Laboratories). Endotoxin was removed using EndoClean reagent (BioVintage). Recombinant Antigen 85B was considered endotoxin-free when it was determined to contain <0.1 EU/ml as assessed by PyroGene Recombinant Factor C Endotoxin Detection System (Cambrex).

**In vitro T cell stimulation assays.** BM-derived macrophages (BMDMs) from C57BL/6 mice were cultured as previously described (38). After 6–7 d of culture, cells were replated at $10^5$ cells/well in flat bottom 96-well plates and treated for 24 h with recombinant mouse IFNγ (20 ng/ml; BD Biosciences). For infection of cultured cells, *M. tuberculosis* H37Rv was grown to an $OD_{580}$ of 0.5–1 in 7H9 broth supplemented with albumin-dextrose-catalase enrichment. A suspension of single bacteria was generated by pelleting the bacteria, resuspending in macrophage culture media, and allowing the bacteria to flow by gravity through a 5-μm syringe filter (Millipore) to remove clumps. Bacteria were enumerated by counting a dilution in a Petroff-Hausser chamber and confirmed by serial dilution and growth on 7H11 agar. BMDMs were incubated with bacteria for 24 h in BMDM growth media. Growth media was removed and extracellular bacteria were removed by washing with PBS. P25TCR-Tg CD4+ T cells were added at $2 \times 10^5$ cells/well in complete media (RPMI, 10% FCS, L-glutamine, nonessential amino acids, sodium pyruvate, Hepes, and β-mercaptoethanol) with or without peptide 25 (custom synthesis by Invitrogen and EZ Biolabs), and cells were incubated for 1–5 d. Supernatants of triplicate wells were pooled and assayed for IFNγ by ELISA (BD Biosciences) and read on a Bio Tek EXL800 plate reader, or proliferation of CFSE-labeled P25TCR-Tg/$Rag1^{-/-}$ CD4+ T cells was assessed by flow cytometry.

**P25TCR-Tg CD4+ T cell isolation and labeling.** P25TCR-Tg mice between 8–16 wk of age were killed according to approved laboratory animal procedures. Lymph nodes and spleen were aseptically removed, and tissues were disrupted by forcing them through a 70-μm cell strainer (BD Biosciences) in RPMI, 5% FCS, 10 mM Hepes. Red blood cells were removed using ACK lysis buffer (155 mM $NH_3Cl$, 10 mM $KHCO_3$, and 88 μM EDTA). Live cells were counted in a hemacytometer using trypan blue exclusion. CD4+ T cells were magnetically isolated using a CD4+ T Cell Isolation kit and an AutoMACS (Miltenyi Biotech). CD4+ T cell purity was routinely >90% as assessed by flow cytometry. For proliferation assays, CD4+ T cells were labeled with CFSE by resuspending the P25TCT-Tg CD4+ cells at a density of $10^7$ cells/ml in room temperature PBS containing 1 μM CFSE (CFDA-SE; Invitrogen). Cells were incubated with CFSE for 7 min at 37°C.

Labeling was stopped with an excess of FCS and the cells were washed three times with RPMI with 10% FCS.

**Adoptive transfer and infection.** CD45.1 mice routinely received 3–5 × $10^6$ CFSE-labeled $CD4^+$ P25TCR-Tg $CD4^+$ T cells (CD45.2) by tail vein injection in 100 μl of sterile PBS. After 24 h, mice were infected by the aerosol route using an Inhalation Exposure Unit (Glas-Col), as previously described (13). The infectious dose was confirmed by killing 4–5 mice within 24 h, and then removing the lungs, forcing them through a 70-μm cell strainer (BD Biosciences), and plating the homogenate on 7H11 agar. Plates were incubated at 37°C, and colonies were counted 14–21 d later.

**Tissue processing and flow cytometry.** At designated time points, 3–5 infected mice in each group were killed, and tissues were used to prepare single-cell suspensions, as previously described (13), with the exception that enzyme digestion was omitted when tissues were used only for T cell isolation. 5 × $10^6$ cells were stained with anti-CD4, anti-CD45.2, and other surface marker antibodies at a density of 1.5 × $10^7$ cells/ml in FACS buffer (PBS, 1% FCS, 0.1% sodium azide, and 1 mM EDTA) and incubated at 4°C for 20–30 min. Cells were washed and fixed in 1% PFA overnight at 4°C. Data were acquired on either a FACSCalibur or LSRII (BD Biosciences). Flow cytometry antibodies were purchased from BD Biosciences or BioLegend. The number of cells of a specific phenotype was determined by taking the percentage of that cell type determined by flow cytometry multiplied by the number of total cells. "Percent proliferating" was defined as the percentage of all P25TCR-Tg $CD4^+$ T cells that had undergone at least one cycle of replication. "Percent divided" was defined as the percentage of the original number of P25TCR-Tg $CD4^+$ T cells that have begun to proliferate assuming no cell death, calculated by FlowJo (Tree Star, Inc.) proliferation platform.

**Detection of IFNγ-producing cells by intracellular cytokine staining.** Single-cell suspensions of lung and lymph node were prepared as in the previous section. Cells were plated at $10^6$ cells per well in a round-bottom 96-well tissue culture plate (Corning) in complete media. 5–7 wells of cells were plated for each mouse and incubated with or without 10 μg of peptide 25 per well for 4–6 h in the presence of Brefeldin A at 37°C with 5% $CO_2$. Cells were stained for the surface markers CD4 and CD45.2 for 30 min at 4°C, followed by fixation for 2 h at 4°C in 2% PFA. IFNγ was detected using Cytofix/Cytoperm kit (BD Biosciences) according to the manufacturer's instructions. Data were acquired on an LSR-II flow cytometer using FACSDiva Software (BD Biosciences) and analyzed using FlowJo software.

**Determination of bacterial load.** At every time point, each tissue from each mouse was assessed for bacterial load by taking an aliquot of the total tissue homogenate before any washing. The aliquot was serial diluted and plated on 7H11 agar. Plates were incubated at 37°C and colonies were counted 14–21 d later. Total colony forming units were determined based on the total volume of tissue homogenate.

**Intranasal and subcutaneous immunization with recombinant Antigen 85B.** *M. tuberculosis*–infected or uninfected mice were anesthetized with a mixture of ketamine and xylazine administered i.p., and given sterile PBS with or without 50 ng of endotoxin-free recombinant Antigen 85B in 30–50 μl of sterile PBS, together with 1 μg of LPS for intranasal immunization or in an emulsion of TiterMax adjuvant (Sigma-Aldrich) for subcutaneous immunization. 3 d after immunization, tissues were harvested and single-cell suspensions were analyzed by flow cytometry and plated for cfu, as described above.

**Online supplemental material.** An analysis of the in vitro response of P25TCR-Tg T cells to Antigen 85B, peptide 25, and *M. tuberculosis*–infected cells can be found in Fig. S1. Fig. S2 shows the P25TCR-Tg T cell responses to intranasal and subcutaneous immunization with Ag85B, demonstrating that the transgenic T cells do not display inherently delayed responsiveness. The expression patterns of CD69, CD25, and IFNγ on P25TCR-Tg T cells over the course of the infection in the lung and mediastinal lymph node are depicted in Fig. S3. In addition, Fig. S3 shows the expression of IFNγ relative to the number of cycles of P25TCR-Tg proliferation in the lung and mediastinal lymph node. The online version of this article is available at http://www.jem.org/cgi/content/full/jem.20071367/DC1.

We thank Dan Littman and members of his laboratory for the use of their LSR-II flow cytometer, and Dr. Mark Eggena for providing training in techniques used for T cell adoptive transfer techniques.

Supported by National Institutes of Health R01-AI051242, and by Strategic cooperation to control emerging and reemerging infections funded by the Special Coordination Funds for Promoting Science and Technology of the Ministry of Education, Culture, Sports, Science and Technology.

The authors have no conflicting financial interests.

**Submitted: 5 July 2007**
**Accepted: 20 November 2007**

## REFERENCES

1. Mogues, T., M.E. Goodrich, L. Ryan, R. LaCourse, and R.J. North. 2001. The relative importance of T cell subsets in immunity and immunopathology of airborne *Mycobacterium tuberculosis* infection in mice. *J. Exp. Med.* 193:271–280.
2. Perlman, D.C., W.M. El-Sadr, E.T. Nelson, J.P. Matts, E.E. Telzak, N. Salomon, K. Chirgwin, and R. Hafner. 1997. Variation of chest radiographic patterns in pulmonary tuberculosis by degree of human immunodeficiency virus-related immunosuppression. *Clin. Infect. Dis.* 25:242–246.
3. Poulsen, A. 1950. Some clinical features of tuberculosis I. Incubation period. *Acta Tuberc. Pneumol. Scand.* 24:311–346.
4. Wallgren, A. 1948. The time-table of tuberculosis. *Tubercle.* 29:245–251.
5. Chackerian, A.A., J.M. Alt, T.V. Perera, C.C. Dascher, and S.M. Behar. 2002. Dissemination of *Mycobacterium tuberculosis* is influenced by host factors and precedes the initiation of T-cell immunity. *Infect. Immun.* 70:4501–4509.
6. Baron, S.D., R. Singh, and D.W. Metzger. 2007. Inactivated *Francisella tularensis* live vaccine strain protects against respiratory tularemia by intranasal vaccination in an immunoglobulin A-dependent fashion. *Infect. Immun.* 75:2152–2162.
7. Chakravarty, S., I.A. Cockburn, S. Kuk, M.G. Overstreet, J.B. Sacci, and F. Zavala. 2007. CD8(+) T lymphocytes protective against malaria liver stages are primed in skin-draining lymph nodes. *Nat. Med.* 13:1035–1041.
8. Kursar, M., K. Bonhagen, A. Kohler, T. Kamradt, S.H.E. Kaufmann, and H.-W. Mittrucker. 2002. Organ-specific CD4+ T cell response during *Listeria monocytogenes* infection. *J. Immunol.* 168:6382–6387.
9. Lira, R., M. Doherty, G. Modi, and D. Sacks. 2000. Evolution of lesion formation, parasitic load, immune response, and reservoir potential in c57bl/6 mice following high- and low-dose challenge with *Leishmania major. Infect. Immun.* 68:5176–5182.
10. McSorley, S.J., S. Asch, M. Costalonga, R.L. Reinhardt, and M.K. Jenkins. 2002. Tracking *Salmonella*-specific CD4 T cells in vivo reveals a local mucosal response to a disseminated infection. *Immunity.* 16: 365–377.
11. Moskophidis, D., and D. Kioussis. 1998. Contribution of virus-specific $CD8^+$ cytotoxic T cells to virus clearance or pathologic manifestations of influenza virus infection in a T cell receptor transgenic mouse model. *J. Exp. Med.* 188:223–232.
12. Srinivasan, A., J. Foley, R. Ravindran, and S.J. McSorley. 2004. Low-dose Salmonella infection evades activation of flagellin-specific CD4 T cells. *J. Immunol.* 173:4091–4099.
13. Wolf, A.J., B. Linas, G.J. Trevejo-Nunez, E. Kincaid, T. Tamura, K. Takatsu, and J.D. Ernst. 2007. *Mycobacterium tuberculosis* infects dendritic cells with high frequency and impairs their function in vivo. *J. Immunol.* 179:2509–2519.
14. Parish, C.R. 1999. Fluorescent dyes for lymphocyte migration and proliferation studies. *Immunol. Cell Biol.* 77:499–508.
15. Gudmundsdottir, H., A.D. Wells, and L.A. Turka. 1999. Dynamics and requirements of T cell clonal expansion in vivo at the single-cell level: effector function is linked to proliferative capacity. *J. Immunol.* 162:5212–5223.

16. Matloubian, M., C.G. Lo, G. Cinamon, M.J. Lesneski, Y. Xu, V. Brinkmann, M.L. Allende, R.L. Proia, and J.G. Cyster. 2004. Lymphocyte egress from thymus and peripheral lymphoid organs is dependent on S1P receptor 1. *Nature*. 427:355–360.
17. Ahmed, R., and D. Gray. 1996. Immunological memory and protective immunity: understanding their relation. *Science*. 272:54–60.
18. Rivera, A., G. Ro, H.L. Van Epps, T. Simpson, I. Leiner, D.B. Sant'Angelo, and E.G.P. Am. 2006. Innate immune activation and CD4+ T cell priming during respiratory fungal infection. *Immunity*. 25:665–675.
19. Foulds, K.E., and H. Shen. 2006. Clonal competition inhibits the proliferation and differentiation of adoptively transferred TCR transgenic CD4 T cells in response to infection. *J. Immunol.* 176:3037–3043.
20. Hataye, J., J.J. Moon, A. Khoruts, C. Reilly, and M.K. Jenkins. 2006. Naive and memory CD4+ T cell survival controlled by clonal abundance. *Science*. 312:114–116.
21. Lee, B.Y., and M.A. Horwitz. 1995. Identification of macrophage and stress-induced proteins of *Mycobacterium tuberculosis*. *J. Clin. Invest.* 96:245–249.
22. Harth, G., B.Y. Lee, J. Wang, D.L. Clemens, and M.A. Horwitz. 1996. Novel insights into the genetics, biochemistry, and immunocytochemistry of the 30-kilodalton major extracellular protein of *Mycobacterium tuberculosis*. *Infect. Immun.* 64:3038–3047.
23. Havlir, D.V., R.S. Wallis, W.H. Boom, T.M. Daniel, K. Chervenak, and J.J. Ellner. 1991. Human immune response to *Mycobacterium tuberculosis* antigens. *Infect. Immun.* 59:665–670.
24. Shi, L., Y.-J. Jung, S. Tyagi, M.L. Gennaro, and R.J. North. 2003. Expression of Th1-mediated immunity in mouse lungs induces a *Mycobacterium tuberculosis* transcription pattern characteristic of nonreplicating persistence. *Proc. Natl. Acad. Sci. USA*. 100:241–246.
25. Mora, J.R., and U.H. von Andrian. 2006. T-cell homing specificity and plasticity: new concepts and future challenges. *Trends Immunol.* 27:235–243.
26. Westermann, J., E.M. Ehlers, M.S. Exton, M. Kaiser, and U. Bode. 2001. Migration of naive, effector and memory T cells: implications for the regulation of immune responses. *Immunol. Rev.* 184:20–37.
27. Ting, L.-M., A.C. Kim, A. Cattamanchi, and J.D. Ernst. 1999. *Mycobacterium tuberculosis* Inhibits IFN-{gamma} transcriptional responses without inhibiting activation of STAT1. *J. Immunol.* 163:3898–3906.
28. Kincaid, E.Z., and J.D. Ernst. 2003. *Mycobacterium tuberculosis* exerts gene-selective inhibition of transcriptional responses to IFN-{gamma} without inhibiting STAT1 function. *J. Immunol.* 171:2042–2049.
29. Fortune, S.M., A. Solache, A. Jaeger, P.J. Hill, J.T. Belisle, B.R. Bloom, E.J. Rubin, and J.D. Ernst. 2004. *Mycobacterium tuberculosis* inhibits macrophage responses to IFN-{gamma} through myeloid differentiation factor 88-dependent and -independent mechanisms. *J. Immunol.* 172:6272–6280.
30. Arko-Mensah, J., E. Julian, M. Singh, and C. Fernandez. 2007. TLR2 but not TLR4 signalling is critically involved in the inhibition of IFN-gamma-induced killing of mycobacteria by murine macrophages. *Scand. J. Immunol.* 65:148–157.
31. Noss, E.H., C.V. Harding, and W.H. Boom. 2000. *Mycobacterium tuberculosis* Inhibits MHC Class II antigen processing in murine bone marrow macrophages. *Cell. Immunol.* 201:63–74.
32. Noss, E.H., R.K. Pai, T.J. Sellati, J.D. Radolf, J. Belisle, D.T. Golenbock, W.H. Boom, and C.V. Harding. 2001. Toll-like receptor 2-dependent inhibition of macrophage class II MHC expression and antigen processing by 19-kDa lipoprotein of *Mycobacterium tuberculosis*. *J. Immunol.* 167:910–918.
33. Fulton, S.A., S.M. Reba, R.K. Pai, M. Pennini, M. Torres, C.V. Harding, and W.H. Boom. 2004. Inhibition of major histocompatibility complex ii expression and antigen processing in murine alveolar macrophages by mycobacterium bovis BCG and the 19-kilodalton mycobacterial lipoprotein. *Infect. Immun.* 72:2101–2110.
34. Comstock, G.W., V.T. Livesay, and S.F. Woolpert. 1974. The prognosis of positive tuberculin reation in childhood and adolescence. *Am. J. Epidemiol.* 99:131–138.
35. Daley, C.L., P.M. Small, G.F. Schecter, G.K. Schoolnik, R.A. McAdam, W.R. Jacobs, and P.C. Hopewell. 1992. An outbreak of tuberculosis with accelerated progression among persons infected with the human immunodeficiency virus. An analysis using restriction-fragment-length polymorphisms. *N. Engl. J. Med.* 326:231–235.
36. Tamura, T., H. Ariga, T. Kinashi, S. Uehara, T. Kikuchi, M. Nakada, T. Tokunaga, W. Xu, A. Kariyone, T. Saito, et al. 2004. The role of antigenic peptide in CD4+ T helper phenotype development in a T cell receptor transgenic model. *Int. Immunol.* 16:1691–1699.
37. Bardarov, S., S. Bardarov Jr., M.S. Pavelka Jr., V. Sambandamurthy, M. Larsen, J. Tufariello, J. Chan, G. Hatfull, and W.R. Jacobs Jr. 2002. Specialized transduction: an efficient method for generating marked and unmarked targeted gene disruptions in *Mycobacterium tuberculosis*, M. bovis BCG and M. smegmatis. *Microbiology*. 148:3007–3017.
38. Banaiee, N., E.Z. Kincaid, U. Buchwald, W.R. Jacobs Jr., and J.D. Ernst. 2006. Potent inhibition of macrophage responses to IFN-{gamma} by live virulent *Mycobacterium tuberculosis* is independent of mature mycobacterial lipoproteins but dependent on TLR2. *J. Immunol.* 176:3019–3027.

Tohoku J. Exp. Med., 2008, **216**, 363-370

# Higher Susceptibility of Type 1 Diabetic Rats to *Mycobacterium tuberculosis* Infection

ISAMU SUGAWARA[1] and SATORU MIZUNO[1]

[1]Mycobacterial Reference Center, The Research Institute of Tuberculosis, Japan Anti-Tuberculosis Association, Tokyo, Japan

An association between diabetes mellitus and tuberculosis has been implicated for a long time. We have previously reported that Goto Kakizaki type 2 diabetic rats are highly susceptible to *Mycobacterium (M.) tuberculosis* infection. As a next step, we attempted to clarify whether type 1 diabetic rats are more susceptible to *M. tuberculosis* than non-diabetic wild-type (WT) rats. Here, we used the Komeda diabetes-prone (KDP) rat, as a model of type 1 diabetes mellitus. The infected KDP rats developed large granulomas without central necrosis in their lungs, liver or spleen. This was consistent with a significant increase in the number of colony-forming units (cfu) of *M. tuberculosis* in the lungs and spleen ($p < 0.01$). Insulin treatment resulted in significant reduction of tubercle bacilli in the infected KDP rats ($p < 0.01$). Pulmonary levels of interferon-$\gamma$, tumor necrosis factor-$\alpha$ and interleukin-1$\beta$ mRNAs were higher in the infected diabetic rats than in WT rats. Alveolar macrophages from KDP rats were not fully activated by *M. tuberculosis* infection because the macrophages did not secrete nitric oxide (NO) that can kill *M. tuberculosis* ($p < 0.01$), but no significant difference in phagocytosis of tubercle bacilli by alveolar macrophages was observed between KDP and WT rats. Taken together, our findings indicate that type 1 diabetic rats are more susceptible to *M. tuberculosis* that WT rats.

——— type 1 diabetic rat; type 1 diabetes mellitus; tuberculosis; cytokine.

Tohoku J. Exp. Med., 2008, **216** (4), 363-370.



Patients with diabetes mellitus (DM) seem to be at high risk of developing tuberculosis, and DM is one of the risk factors for tuberculosis. It has been implicated that there is a clinical link between diabetes mellitus and pulmonary tuberculosis (Garay 2004), and several studies have investigated this issue (Banyai 1931; Root 1934; Boucot et al. 1952; Kim et al. 1995). As patients with DM are increasing worldwide, it is important to examine why diabetic patients are susceptible to *M. tuberculosis* infection.

DM is broadly classified into two types: type 1 (insulin-dependent) and type 2 (insulin-independent) (Powers 2008). There are several animal models of DM including non-obese diabetic (NOD) mice and spontaneously diabetic Goto Kakizaki (GK) rats (Goto et al. 1976; Makino et al. 1976). When GK rats were used to examine the relationship between type 2 DM and tuberculosis, we found that the rats developed large granulomas and that their alveolar macrophages were not fully activated by *Mycobacterium (M.) tuberculosis* infection (Sugawara et al. 2004). This was consistent with the significantly increased

Received August 21, 2008; revision accepted for publication November 11, 2008.

Correspondence: Dr. Isamu Sugawara, Mycobacterial Reference Center, The Research Institute of Tuberculosis, 3-1-24 Matsuyama, Kiyose, Tokyo 204-0022, Japan.
e-mail: sugawara@jata.or.jp

number of colony-forming units of *M. tuberculosis* in the lung and spleen tissues.

We then examined the relationship between type 1 DM and experimental tuberculosis. As at the time there was no rat model of type 1 diabetes, NOD type 1 mice were utilized instead for this purpose. The results were variable and inconsistent. NOD mice developed large granulomas in one experiment, but not in another experiment. It has been reported previously that NOD mice are resistant to *M. avium* and that the infection prevents autoimmune disease (Bras and Aguas 1996). Moreover, protection of NOD mice from diabetes is a Th1-type response that is mediated by up-regulation of the Fas-FasL pathway and involves an increase in the cytotoxicity of T cells (Martins and Aguas 1999). Clearly, the pathogenesis of tuberculosis in NOD mice is a complex process and requires further clarification.

A rat model of type1 diabetes was eventually developed in 1998 in Japan, and was named the Komeda diabetes-prone (KDP) rat (Komeda et al. 1998; Yokoi et al. 2003). It is reported that Cblb, a member of the Cbl/Sli family of ubiquitin-protein ligases, is a major susceptibility gene for rat type 1 diabetes mellitus (Yokoi et al. 2002). This research background led us to re-examine the pathophysiology of pulmonary tuberculosis in type 1 diabetic rats. Our results suggest that type 1 diabetic rats are more susceptible to *M. tuberculosis* infection than non-diabetic rats.

## Materials and Methods

*Animals*

Six-week-old female type 1 diabetic rats and sex- and age-matched control Long-Evans Tokushima lean (LETL) rats were purchased from SLC Co. (Shizuoka, Japan) (Komeda et al. 1998). The diabetic rats are not obese and develop insulitis with lymphocyte infiltration over time, being responsive to rabbit insulin, which ameliorates the diabetes. Hyperlipidemia and hypercholesterolemia are not recognized in KDP rats. The blood glucose level in this model was measured with an Ascensia Brio blood glucose measurement apparatus (Bayer Medical Co., Tokyo, Japan) with a measurement range of 30-550 mg/dl. All rats were housed in a biosafety level 3 facility and given rat chow and water *ad libitum* after aerosol infection with *M. tuberculosis* Kurono strain. The degree of severity of type 1 DM in the diabetic rats was evaluated mainly by assessment of blood glucose levels. Blood glucose levels in the rats were between 200 and 550 mg/dl.

*Experimental infections*

The Kurono strain of *M. tuberculosis* (ATCC35812) was grown in Middlebrook 7H9 broth for two weeks, and then filtered with a sterile acrodisc syringe filter with a pore size of 5.0 $\mu$m. Aliquots of the bacterial filtrate were stored at –80°C until use. The diabetic and WT rats were infected via the airborne route by placing them in an exposure chamber in a Glas-Col aerosol generator (Glas-Col, Inc., Terre Haute, IN, USA) (Sugawara et al. 2004). The nebulizer compartment was filled with 5 ml of a suspension containing $3 \times 10^6$ colony-forming units (cfu) of Kurono tubercle bacilli so that approximately 200 bacteria would potentially be deposited in the lungs of each animal. Inhalation infection experiments were carried out twice.

For some experiments, the diabetic rats were treated with 100 $\mu$l rabbit insulin (10 ng/ml, Shibayagi Co., Takasaki, Gunma, Japan) twice daily from the day after aerosol infection. The blood glucose level of the insulin-treated KDP rats was less than 200 mg/dl. Permission to perform the experiments on the animals was granted by the Animal Experiment Committee at the Research Institute of Tuberculosis.

*Colony-forming unit (cfu) assay*

At 7 weeks after aerosol infection, the rats were anesthetized with pentobarbital sodium. The right lobe of each lung and part of the spleen tissue were weighed and used to evaluate the *in vivo* growth of mycobacteria. The lung and spleen tissues were homogenized with a mortar and pestle, and 1 ml of a sterile dilution of the homogenate was cultured on 1% Ogawa egg medium. Colonies were counted after four weeks of incubation at 37°C (Yamada et al. 2001).

*In vitro effect of glucose on mycobacterial growth*

Diabetes is characterized by hyperglycemia. In order to examine the *in vitro* effect of glucose on *M. tuberculosis* growth, 0.1%, 0.5% and 1% glucose (w/v) was added to *M. tuberculosis* Kurono strain in 7H9 medium and the mixture was cultured for one week. Thereafter, the 10-fold-diluted culture suspension was cultured on 1% Ogawa egg medium for four weeks and the colonies

were counted.

*Histopathology*

For light microscopy, the rats were sacrificed seven weeks after infection. Tissue sections were cut from paraffin blocks containing lung, liver or spleen tissue and stained with hematoxylin and eosin or by the Ziehl-Neelsen method for acid-fast bacilli (Sugawara et al. 2004).

*Real-time PCR*

Another portion of the remaining right lower lobes of the lungs was used for reverse transcriptase PCR (RT-PCR) analysis to examine the expression levels of several cytokine mRNAs in these samples during *M. tuberculosis* infection. These samples were snap-frozen in liquid nitrogen and stored at −85°C until use. RNA extraction was performed as described previously (Yamada et al. 2005). Briefly, the frozen tissues were homogenized in a microcentrifuge tube with an autoclaved disposable 1000-$\mu$L tip cooled by dipping in liquid nitrogen. Then the homogenates were treated with 1 mL of TRIzol reagent (Invitrogen Japan Co., Tokyo, Japan), as specified by the manufacturer. After RNA isolation, total RNA concentration was measured with a spectrophotometer, and the agarose gel electrophoresis pattern of the total RNA was examined. The total RNAs were reverse-transcribed into cDNA with Moloney murine leukemia virus reverse transcriptase (Invitrogen). ABI Taqman® Gene Expression Assay was used for relative quantitative measurement of the mRNA expression of interferon (IFN)-$\gamma$, tumor necrosis factor (TNF)-$\alpha$, and interleukin (IL)-1$\beta$ (Yamada et al. 2005). A TaqMan® Rodent GAPDH Control Reagents set was used for normalization for data analysis. Real-time RT-PCR was performed according to the instructions for the ABI PRISM 7900HT Sequence Detection System (Applied BioSystems Inc.). Data were analyzed by the $\Delta\Delta C_T$ method using the ABI PRISM Sequence Detection System software package (version 2.1; Applied BioSystems, California, USA) running on Windows 2000. The results obtained from diabetic and control rats were expressed as relative expression quantities of the targets in comparison with those of non-infected rats that were calibrated with the expression of an internal control gene glyaraldehyde-3-phosphate dehydrogenase (GAPDH) (Yamada et al. 2005; Yamada et al. 2007).

*Alveolar macrophage nitric oxide (NO) assay*

Alveolar macrophages ($3 \times 10^6$/well) were plated in 96-well culture plates in RPMI 1640 (Sigma-Aldridge, St. Louis, MO, USA) supplemented with 10% heat-inactivated fetal calf serum and then stimulated with *M. tuberculosis* Kurono strain and cultured overnight. The supernatants were collected 16 hours after culture seeding, filtered, and their NO concentrations were determined by the Griess assay as described previously (Green et al. 1990; Sugawara et al. 2004).

*Statistical analysis*

All values were expressed as means±S.E. and compared using Student's $t$ test. For all statistical analyses, the level of statistical significance was set at $p < 0.01$.

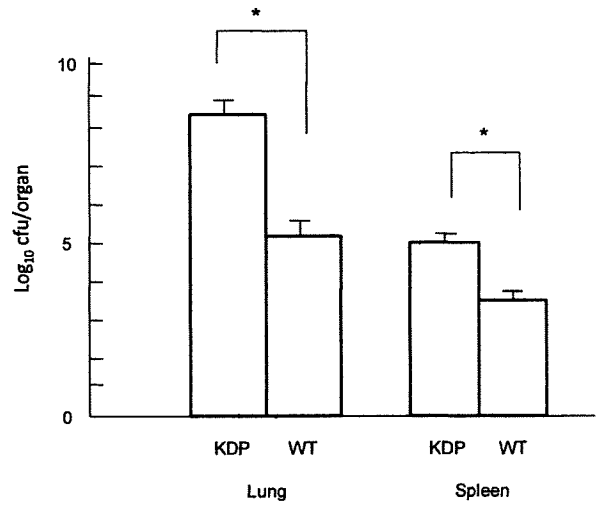


Fig. 1. Mycobacterial burden in the lung and spleen tissue of type 1 diabetic rats.
Colony-forming units (cfu) in lung and spleen tissues from type 1 diabetic (KDP) rats and wild-type rats exposed to $3 \times 10^6$ cfu of *M. tuberculosis* Kurono strain by aerosol infection. Seven weeks after infection, three rats from each group were sacrificed, and homogenates of the lungs and spleen were cultured. There is a significant difference in the lung and spleen cfu counts between KDP and WT rats ($p < 0.01$).
Error bars indicate standard deviation (SD) from the mean. *$p < 0.01$ vs. WT rats.

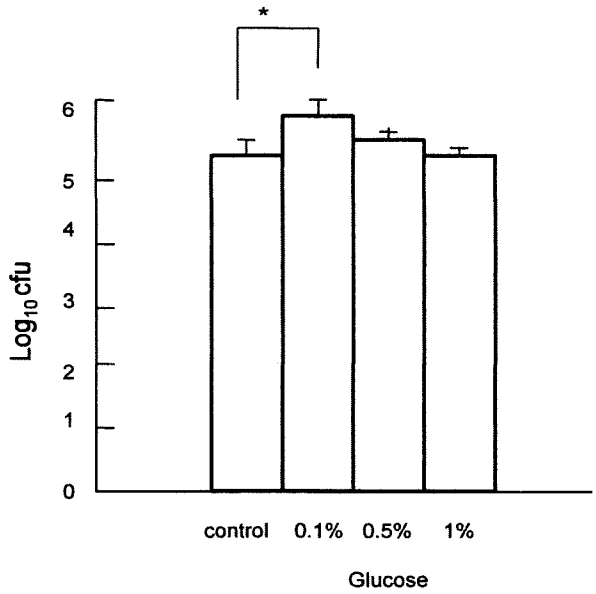


Fig. 2. *In vivo* effect of insulin treatment on tubercle bacilli in granulomas.
Type 1 diabetic (KDP) rats were treated with 100 $\mu$l rabbit insulin (10 ng/ml, Shibayagi Co., Takasaki, Gunma, Japan) twice daily from the day after aerosol infection. *$p < 0.01$ vs. WT rats.

## Results

### *Mycobacterial burden in the lung and spleen tissue of KDP rats*

When diabetic and WT LETL rats were infected via the airborne route with the Kurono strain of *M. tuberculosis* ($3 \times 10^6$), all rats survived until the date of sacrifice (49 days after infection). As shown in Fig. 1, the number of mycobacterial colonies in the lung and spleen tissues increased, and there was a significant difference in the lung and spleen cfu counts between diabetic and WT rats ($p < 0.01$).

When insulin was administered to the diabetic rats subcutaneously twice daily, it reduced pulmonary and splenic cfu counts significantly ($p < 0.01$) and their cfu counts were similar to those in WT rats (Fig. 2).

### *Histopathology of infection*

When $3 \times 10^6$ cfu of the Kurono strain was given to the rats via the airborne route, larger granulomas were recognized in the lungs of the diabetic rats than in the WT controls (Fig. 3A). No Langerhans-like multinucleated giant cells were found in the granulomatous lesions. No necrotic lesions were present in these granulomas. The pulmonary granulomas merged with the surrounding granulomas over time, and foamy epithelioid macrophages were more prominent. Although no tubercle bacilli were noted in the pulmonary granulomas of WT rats, acid-fast tubercle bacilli were more prominent in the granulomas of diabetic rats (Fig. 3B). Small granulomas were recognized in the spleen and liver of diabetic rats. Conversely, the granulomas of WT rats were discrete and isolated (Fig. 3C).

The diabetic rats, which were given insulin twice daily after infection, were dissected histologically. The sizes of pulmonary granulomas in the insulin-treated diabetic rats were found to be reduced significantly (Fig. 3D).

### *In vitro effect of glucose on mycobacterial growth*

Three different concentrations of glucose were added to *M. tuberculosis* in 7H9 liquid medium. Mycobacterial growth was concentration-dependent (Fig. 4), and maximal when 0.1% glucose was added to the tubercle bacilli ($p < 0.01$). Although 0.5% glucose also increased mycobacterial growth, the difference between 0.5% glucose and no addition was not statistically significant. Addition of 1% glucose did not induce growth of tubercle bacilli significantly (Fig. 4).

### *Real-time PCR*

The data thus obtained were expressed as relative intensity (Fig. 5). In the lung tissues of non-infected KDP and WT rats, the expression levels of IFN-$\gamma$, TNF-$\alpha$ and IL-1$\beta$ mRNA were very low (< 0.1 as relative intensity). The expression of pulmonary IFN-$\gamma$ mRNA was higher at 7 weeks after infection in the infected diabetic rats than in control rats, the mRNA expression in the former being > 3 times that in the latter ($p < 0.01$). Pulmonary TNF-$\alpha$ mRNA expression in the infected diabetic rats was 4 times higher than in the infected control rats ($p < 0.01$). On the other

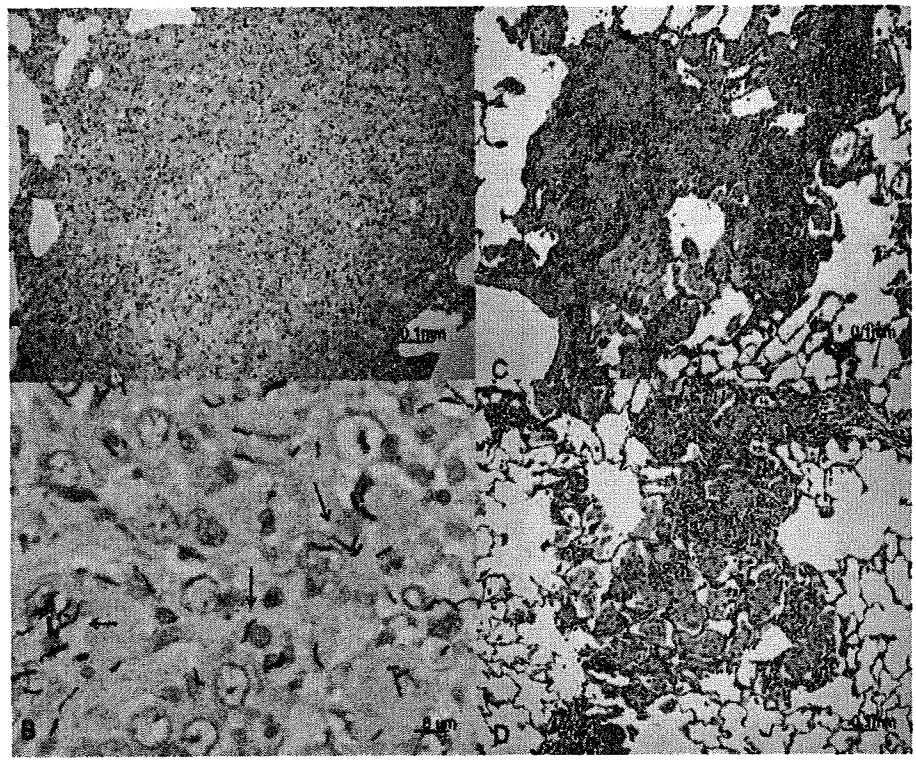

Fig. 3. Histopathology of the infected lung tissue.
Formalin-fixed sections were stained with hematoxylin and eosin (A, C and D) and Ziehl-Neelsen stain for acid-fast bacilli (→) (B).
(A) Pulmonary tissue from a diabetic type 1 (KDP) rat infected with the Kurono strain (7 weeks after infection)(magnification, × 100). (B) Pulmonary tissue from a KDP rat infected with the Kurono strain 7 weeks after infection (magnification, × 500) (C) Pulmonary tissue from a wild-type (WT) rat infected with the Kurono strain (7 weeks after infection)(magnification, × 100). (D) Pulmonary tissue from a KDP rat infected with the Kurono strain and treated with insulin twice daily (7 weeks after infection) (magnification, × 100). Larger granulomas were recognized in the lungs of KDP rats than in the WT controls (A). The sizes of pulmonary granulomas in the insulin-treated KDP rats were reduced significantly (D).

hand, the pattern of expression of pulmonary IL-1$\beta$ mRNA was slightly different, and two times higher than in the infected controls.

*Nitric oxide (NO) assay*

NO levels in the culture supernatants of alveolar macrophages were determined using Griess reagent with reference to a standard $NaNO_2$ curve. The levels of NO produced by unstimulated alveolar macrophages from both KDP and WT rats were < 20 $\mu$M. However, when the alveolar macrophages were stimulated overnight with the Kurono strain (multiplicity of infection=10), NO levels increased to 65 ± 5 $\mu$M (control rats) and 25 ± 2 $\mu$M (type 1 diabetic rats). The difference in NO secretion capacity between diabetic and WT rats was statistically significant ($p < 0.01$) (Table 1).

## Discussion

In this study, large granulomas were induced in rats with type 1 diabetes after aerosol infection with *M. tuberculosis*. The number of cfu in lung and spleen tissues taken from the diabetic rats was significantly higher than that in WT control rats ($p < 0.01$). Similar findings were obtained when the experiments were repeated.

Although central necrosis was not recog-